General circulation of the western subtropical North Atlantic observed using profiling floats

Young-Oh Kwon[1] and Stephen C. Riser

School of Oceanography, University of Washington, Seattle, Washington, USA

[1]   The general circulation of the subtropical western North Atlantic is described using hydrography and subsurface velocity measured simultaneously by 71 profiling floats during the period July 1997 to December 2002. Subsurface trajectories of the floats revealed a strong topographic influence and depth-dependence of the Gulf Stream, its recirculation gyres, and the North Atlantic Current. We discuss eddy-like and nonsteady flows in several subregions, especially near the major topographic features. The seasonal cycle of volume transport, estimated using the absolute geostrophic velocity in the upper 900 m, was shown to be a maximum in winter and minimum in summer. The eddy kinetic energy and eddy diffusivity, derived from the float data and mapped over the subtopical gyre, show seasonal variability in the vicinity of the Gulf Stream with a maximum in spring and minimum in winter for both quantities.

Citation: Kwon, Y.-O., and S. C. Riser (2005), General circulation of the western subtropical North Atlantic observed using profiling floats, *J. Geophys. Res.*, *110*, C10012, doi:10.1029/2005JC002909.

1. Introduction

[2]   Describing the general circulation of the ocean has traditionally been the most fundamental scientific problem in physical oceanography. Numerous studies have focused on understanding circulation of the subtropical North Atlantic since *Iselin*'s [1936] seminal synthesis. Traditionally, the dynamic method, based on shipboard hydrographic observations, has generally been used to derive the general circulation [e.g., *Worthington*, 1976; *Stommel et al.*, 1978; *Reid*, 1978; *Lozier et al.*, 1995], despite the uncertainty for the choice of a reference level. Alternatively, float measurements have been widely used to describe the circulation based on direct velocity estimation, as by *Rossby et al.* [1983], *Richardson* [1983], *Frantantoni* [2001], *Reverdin et al.* [2003], and *Owens* [1991]. The use of satellite altimetry to estimate the surface geostrophic velocity and the eddy variability has rapidly increased during the last decade [*Wunsch and Stammer*, 1998; *Ducet et al.*, 2000]. A limitation on both the float methods and the satellite altimetry is that their information is confined to one fixed surface, the float drift depth for the floats or the sea surface for the altimeter. To overcome the limitations of a single method, several attempts have been made to combine the dynamic method with either float observations [*Lavender et al.*, 2000; *Perez-Brunius et al.*, 2004] or altimeter data [*Qiu*, 1994], as a level of known motion. Potential incompatibility between the data sets can be a problem for mapping the basin-wide or gyre-scale velocity field using the merged methods.

[3]   In this work we present data observed by profiling floats in the subtropical North Atlantic and attempt to use the simultaneous observations of velocity and hydrographic properties to yield an estimate of the absolute geostrophic velocity field of the ocean at depths above 1000 m. The subtropical North Atlantic is arguably the most highly studied of any region in the world ocean, at least by physical oceanographers, and there are surely hundreds of studies of the general circulation in this region. Our results are not inconsistent with the bulk of those studies, but the results derived here do allow for vastly better spatial and temporal coverage than most previous efforts and do not depend on ad hoc assumptions concerning a reference level (our only assumption is that the flow is geostrophic). An introduction of the data and a quasi-Lagrangian description of the subsurface trajectories of the floats will be given in sections 2 and 3 of this paper. The absolute geostrophic velocity for the upper 900 m of the subtropical North Atlantic is presented in section 4. The seasonal variability of volume transport derived from the absolute velocity is discussed in section 5. Finally, the seasonal eddy variability at 900 m and a summary are given in sections 6 and 7.

2. Data

[4]   Observations of temperature and salinity profiles and subsurface velocities collected by profiling floats were used to describe the general circulation of the study region (Figure 1). Profiling float technology has been discussed

---

[1]Now at Climate and Global Dynamics Division, National Center for Atmospheric Research, Boulder, Colorado, USA.
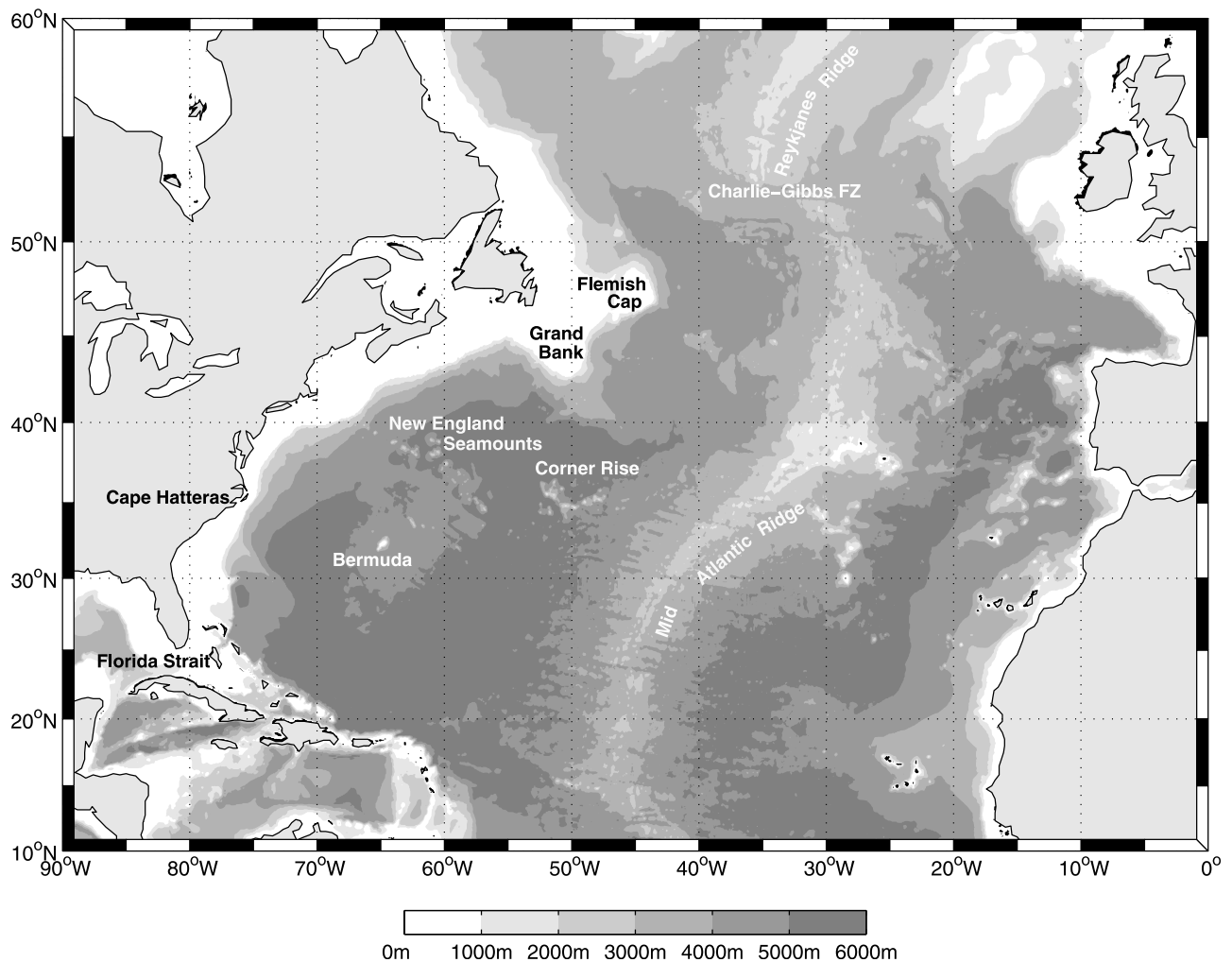
Figure 1. Topographic and geographic features referred to in the text.

in detail by *Roemmich et al.* [2004]. The floats cycle vertically at predetermined intervals, from a depth where they are neutrally buoyant to the sea surface, by actively changing their buoyancy. While at the sea surface, most of the floats are located by, and relay data to, NOAA weather satellites that are equipped to function as part of the ARGOS system. The floats are designed to collect vertical profiles of ocean variables such as temperature and salinity during their periodic ascents. Surface velocity and subsurface velocity at the parking-depth can be inferred from the satellite fixes. The floats used in this study were an early version of profiling floats and were often referred to as PALACE (Profiling Autonomous LAgrangian Circulation Explorer) [*Davis et al.*, 2001] floats.

[5] Beginning in July 1997, 71 profiling floats were deployed in western subtropical region of the North Atlantic ($20°-40°$N, $40°-80°$W) as a part of the Atlantic Circulation and Climate Experiment (ACCE) (see Figure 2). The components for these floats were purchased from Webb Research Corporation, and the construction, checkout, and deployment of the floats were carried out by the University of Washington. The floats were programmed to drift at nominal depth of 1000 m and to ascend to the sea surface at the end of every 10-day period. Temperature was measured at approximately 100 depths between 1000 m and the sea surface during their ascents; 11 floats among the 71 were capable of making salinity measurements as well. The floats spent about 14 hours at the sea surface uploading the data from each profile before descending and beginning the next cycle. More than 8000 temperature-only profiles and 820 CTD profiles were collected during the period July 1997– December 2002 (Figure 3). Concomitantly, more than 240 float-years of parking-depth velocity data were obtained.

[6] All the floats were programmed to drift at a nominal depth of 1000 m, but the first 18 of the 71 floats suffered from gradual shoaling of the parking-depth, with the average rate of about 1.1 m/day (Figure 4). Two independent factors were identified to be responsible for gradual loss of mass that was responsible for the shoaling. One was the ablative antifoulant coating that was painted on a few of the early floats, and the other was the corrosion of the anodized aluminum hull of the unpainted floats. These problems were identified and fixed for the later floats. Shoaling of the
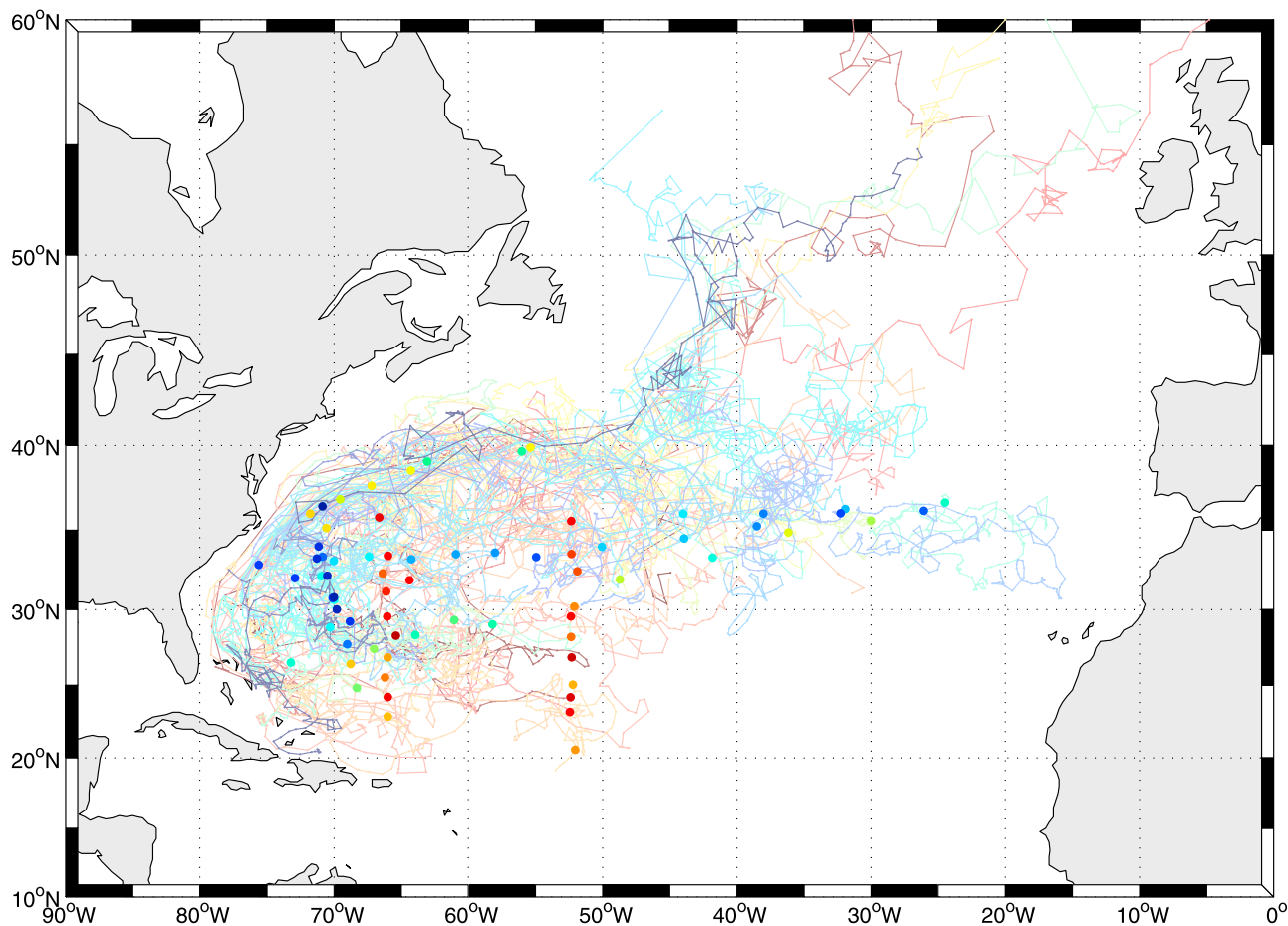
Figure 2. Trajectories of the 71 floats used in this study, during July 1997–December 2002. Bold dots indicate the deployment position for each float. Different colors are assigned to each float. Trajectory and deployment position for each float have the same color.

parking-depth provided trajectories at various depths in the upper 1000 m, which in some ways was a serendipitous benefit.

3. Float Trajectories

[7] In this section we provide a quasi-Lagrangian description of individual float trajectories at the parking-depth for different parts of the study region. The float trajectories were interrupted as the floats ascended to the sea surface every 10 days; thus, only the submerged displacements are plotted in the figures, with a gap in the trajectories indicating the period when the floats were transmitting on the surface. Because of these interruptions, the floats can only be quasi-Lagrangian. The study of *Riser* [1982] suggested that SOFAR floats drifting at depths below the thermocline can be markers of distinct fluid parcels over times perhaps as long as a few months. But here, in the case of profiling floats, where the float essentially follows a new particle every 10 days or so, the interpretation of the float trajectory as a particle trajectory is more problematic. In what follows here we loosely identify float trajectories with the motion of particles at the parking depth, but we do not use this identification in

any quantitative way. Furthermore, it is our interpretation that the float trajectory represents one member of an ensemble of possible particle trajectories from an initial deployment position, but lacking the repeated releases from a given deployment position and the continuous tracking of each float, we cannot know the probability distribution of particle motion.

3.1. Gulf Stream and Southern Recirculation Gyre

[8] Most of the floats drifted within the Gulf Stream and/ or the southern recirculation gyre during some part of their lifetime (Figure 2). Figure 5 presents trajectories of 5 selected floats, showing the typical subtropical gyre. It appears that the gyres tend to be smaller and more confined to the northwestern corner of the region at deeper levels. Additionally, the tracks indicate that bathymetry clearly plays a role as a major constraint for limiting the zonal extent of the gyre [*Richardson*, 1981]: when floats left the Gulf Stream and turned southward into the recirculation gyre there was usually blocking topography such as the New England Seamounts, the Corner Rise, or the Mid Atlantic Ridge.

[9] Float 023 followed the longest path, which extended all the way to the Mid-Atlantic Ridge. It drifted at around
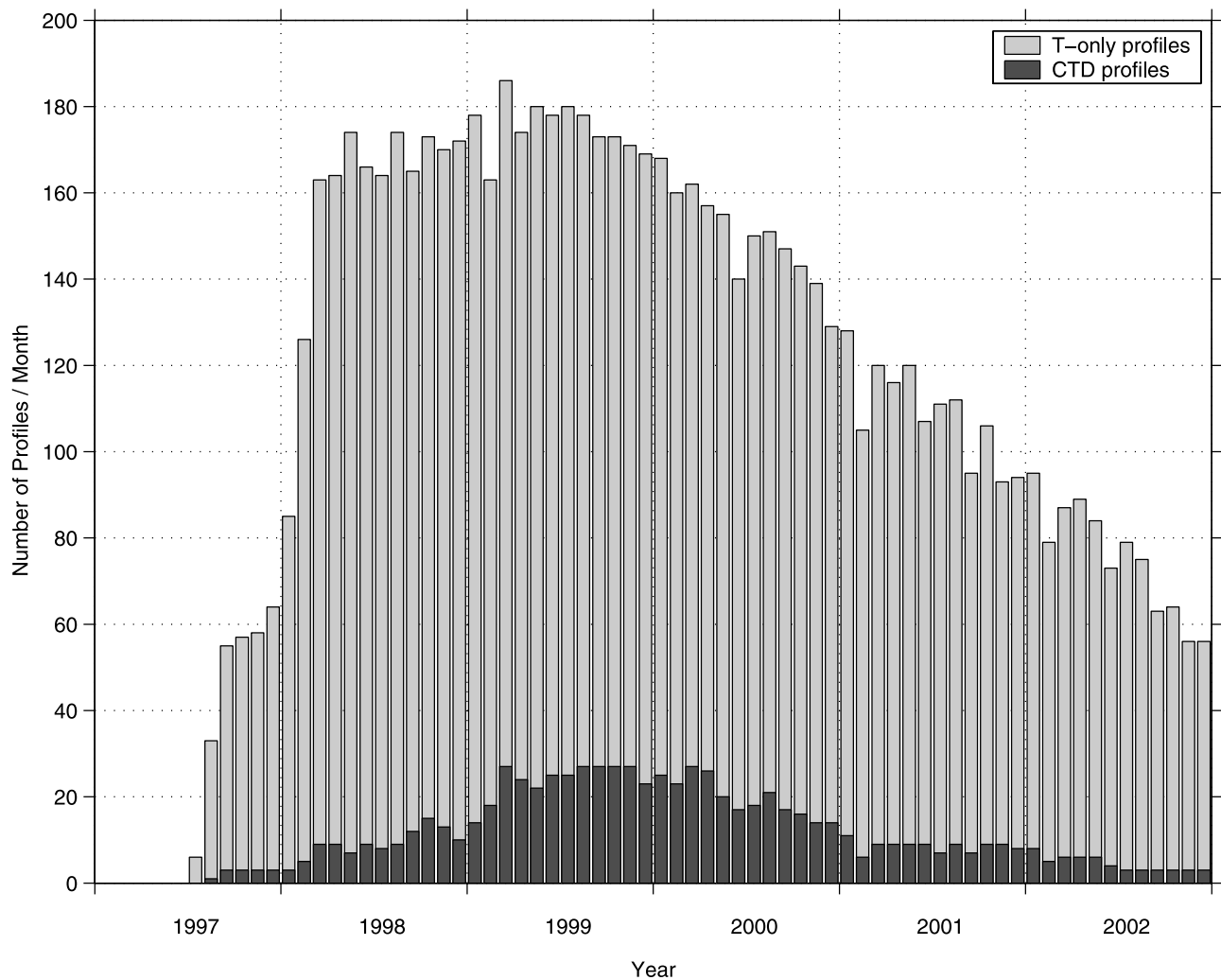
Figure 3. Monthly number of observations for all 71 floats during July 1997–December 2002. Gray bars are for the temperature-only profiles, and the black bars are for the CTD profiles.

300 m depth eastward in the Gulf Stream and headed south along the axis of the Mid-Atlantic Ridge. Float 001 left the Gulf Stream near 47°W and reached the western flank of the Mid-Atlantic Ridge to travel southward at about 400 m depth. Float 024 headed south near the Corner Rise around 50°W at about 400 m depth. Float 114 drifted near 950 m depth, and when blocked by the New England Seamounts turned southward. Float 105 showed the weakest and deepest gyre-scale motion, at about 1050 m depth, which extended only to 67°W.

[10] Entrainment into the Gulf Stream can also be seen in Figure 5. Float 023, shoaling from 1000 m to 500 m along its path, was entrained into a boundary current along the Bahamas. Floats 001, 024, 114 were entrained into a western boundary current near 30°N. Float 105 was entrained into a boundary current at 34°N near the Cape Hatteras, then de-entrained and re-entrained near 30°N. Some trajectories (not shown here) showed frequently repeated entrances and exits from flows along the western boundary, at latitudes between 25°N and 36°N, seemingly consistent with the trajectories of SOFAR floats at 700 m reported by *Rossby et al.* [1983]. Table 1 summarizes the locations of 42 western boundary entrainments observed in the ACCE floats. It clearly demonstrates that there was no single preferred entrainment location but that instead the western boundary current system appears to entrain fluid from the gyre interior all along its length. Of the 42 entrainments, 9 occurred after the Gulf Stream separated from the coast and flowed eastward. Some of these events are described in detail in the later subsection.

3.2. Northern Recirculation Gyre

[11] Several floats followed at least some part of the northern recirculation gyre of the Gulf Stream (Figure 6). Float 080 was deployed almost within the Gulf Stream near 70°W and drifted eastward within the Gulf Stream until it reached 60°W at around 800 m depth, then traveled northward from 39°N, 60°W to 42°N, 59°W and finally moved westward to 68°W along the continental slope almost parallel to the 4000 m isobath. Later it drifted onshore and followed 1000 m bathymetry all the way to 75°W to
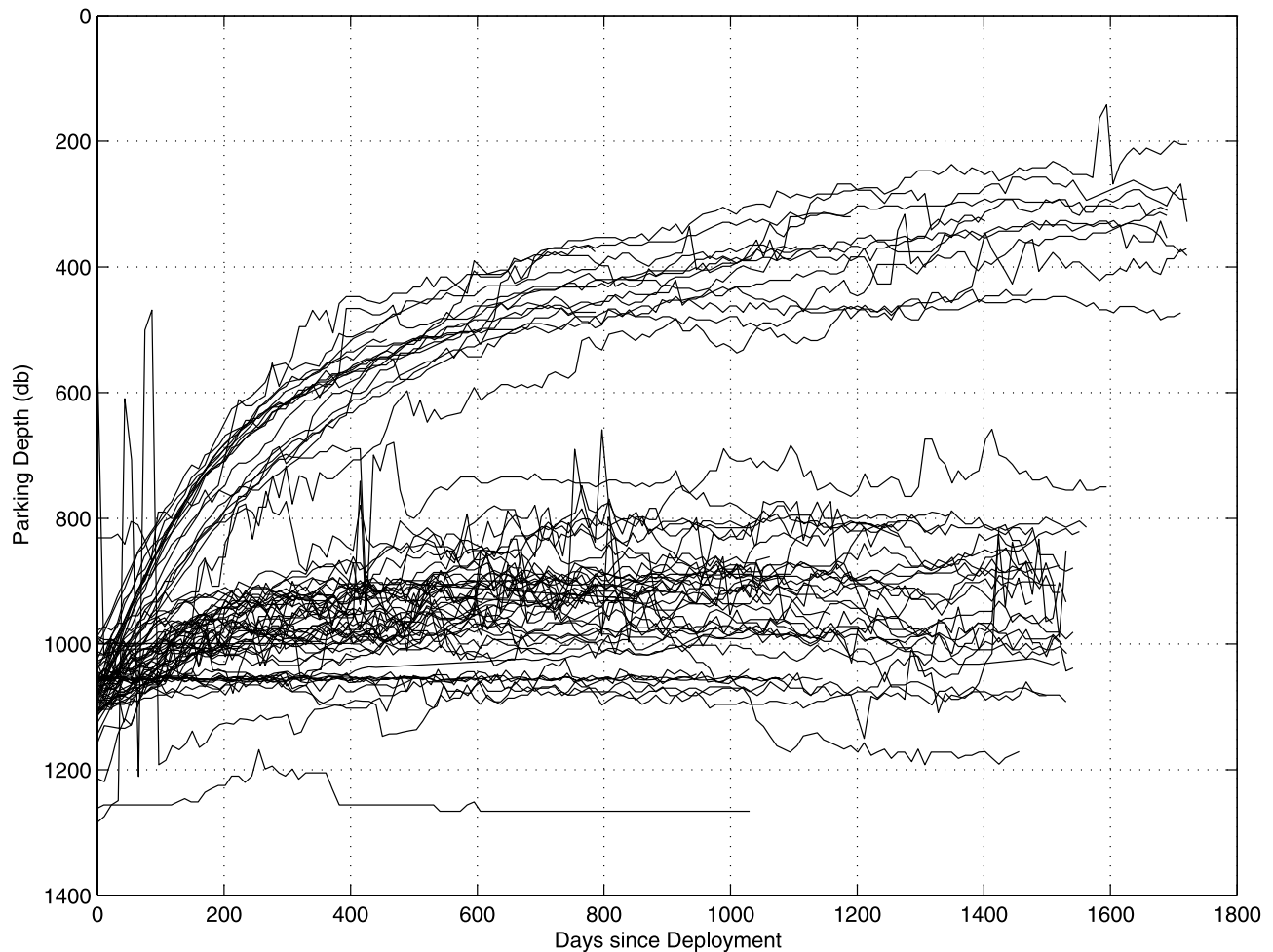
Figure 4. Parking-depths of all 71 floats starting from the deployment of each float. Each line is for single float.

complete the recirculation. After completing the northern recirculation gyre once, the float was re-entrained into the Gulf Stream and later followed the southern recirculation gyre. It took 330 days for Float 080 to travel from the point it was detached from the Gulf Stream to the point of re-entrainment. The mean velocity along the continental slope was about 6 cm/s in the westward direction. Float 019 showed a very similar recirculation gyre except that its eastern limit was 64°W, with the float drifting near a depth of 300 m. The trajectory showed cross isobath drift from the 3000 m isobath to the 1000 m isobath at a similar location as the Float 080.

3.3. Gulf Stream Extension - North Atlantic Current

[12] The Gulf Stream travels eastward as a zonal jet to ~50°W, where it has been proposed to bifurcate into the Azores Current, which continues east, and a northward branch known as the North Atlantic Current [*Clarke et al.*, 1980; *Krauss*, 1986]. There were 23 floats, which reached the tail of the Grand Bank around 50°W, and 9 floats among them entered the subpolar gyre via the North Atlantic Current (Figure 7). The trajectories diverged and were less constrained by the topography after the separation near Cape Hatteras, but most reattached themselves to the

continental slope near the Grand Banks. They drifted northward along the continental slope until they passed the Flemish Cap and followed three different routes. One of the floats (Float 110) drifted northwestward and stayed parallel to the continental slope. This northwestward pathway offshore of the strong southeastward boundary current is known to be part of the weak anticyclonic recirculation along the boundary current in the Labrador Sea [*Lavender et al.*, 2000; *Fischer and Schott*, 2002]. Four floats (Float 082, 094, 113, 228) drifted northwestward until they separated from the western boundary near the Northwest Corner (~50°N, 44°W) [*Rossby*, 1996; *Carr and Rossby*, 2001] and headed eastward into the open ocean. Three floats (Float 004, 013, 026) began to drift eastward and north-eastward into the open ocean around the Flemish Cap. Four floats reached the Northwest Corner drifted around 800–1000 m, while the three floats separated near the Flemish Cap were at around 300–600 m. Float 119 also drifted northeastward into the open ocean, but the exact location of the separation from the western boundary couldn't be recovered due to the failure of the float to surface for 106 days near the Flemish Cap.

[13] Three deeper floats drifted between 800 m and 1000 m (Floats 082, 094, 228), crossed the Mid-Atlantic
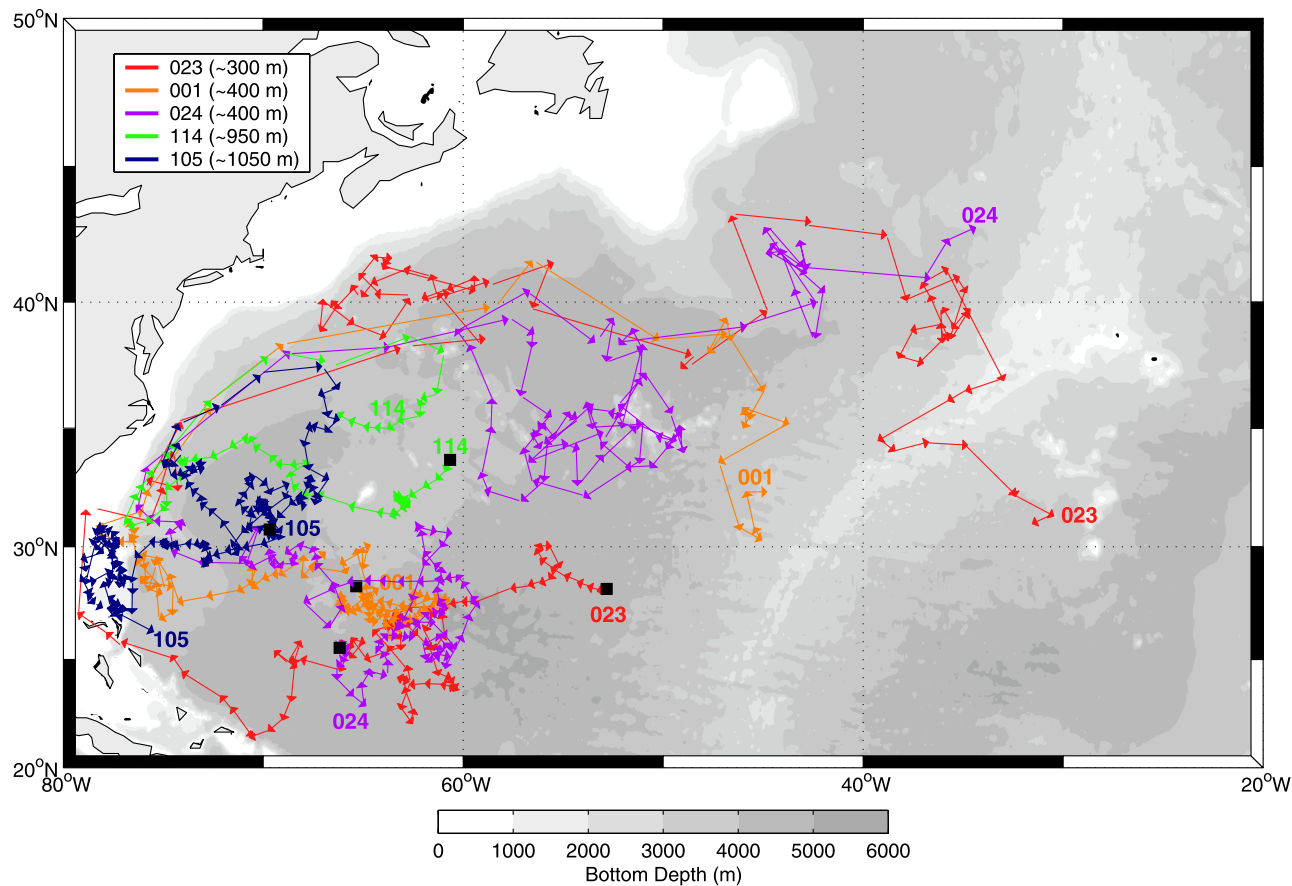
Figure 5. Trajectories of five selected floats that showed the Gulf Stream and various sizes of the southern recirculation gyres. Black squares indicate the deployment location of each float. The numbers indicate the identification number of each float. The trajectory of each float is plotted with different color as specified in the legend. The legend also contains the approximate depth of each float in the parenthesis. Since only the submerged displacement is plotted, the arrows are slightly disconnected. Underlying gray shades show the bathymetry.

Ridge above the Charlie-Gibbs Fracture Zone (~52°N, 32°W) and dispersed into the northeastern North Atlantic. All these floats separated from the western boundary near the Northwest Corner. Float 004 also passed the Mid-Atlantic Ridge at a location slightly south of the Charlie-Gibbs Fracture Zone then made an anti-cyclonic loop to pass the Mid-Atlantic Ridge again through the Faraday Fracture Zone (~50°N, 30°W) at a depth of around 600 m. It took 245–376 days for the above 4 floats to travel from the southeastern corner of the Flemish Cap to the Charlie-Gibbs Fracture Zone, yielding a mean northeastward speed was about 4 cm/s in this depth range. The other the deeper float (Float 113) drifted towards the Charlie-Gibbs Fracture Zone but died before crossing the Mid Atlantic Ridge. These results are in agreement with *Bower et al.* [2002], who showed concentrated eastward flow over the Charlie-Gibbs Fracture Zone from various subsurface floats. Two floats shallower than 300 m (Float 013 and 026) crossed the Mid-Atlantic Ridge further south, near 45°N, a pathway also identifiable from surface drifter trajectories [*Reverdin et al.*, 2003].

Table 1. Number of Entrainments Observed Within Each Segment of the Gulf Stream

| Segment Location	Number of the Observations	Depths of the Observations, m
South of Florida Strait	6	346, 378, 384, 447, 540, 999
Florida Strait - 32°N	12	380, 453, 521, 713, 790, 810, 929, 983, 992, 1035, 1081, 1105
32°N - Cape Hatteras	7	333, 866, 960, 961, 966, 993, 1012
Near Cape Hatteras	8	376, 744, 854, 877, 978, 1015, 1056, 1081
East of Cape Hatteras	9	318, 447, 466, 611, 692, 871, 890, 1053, 1068
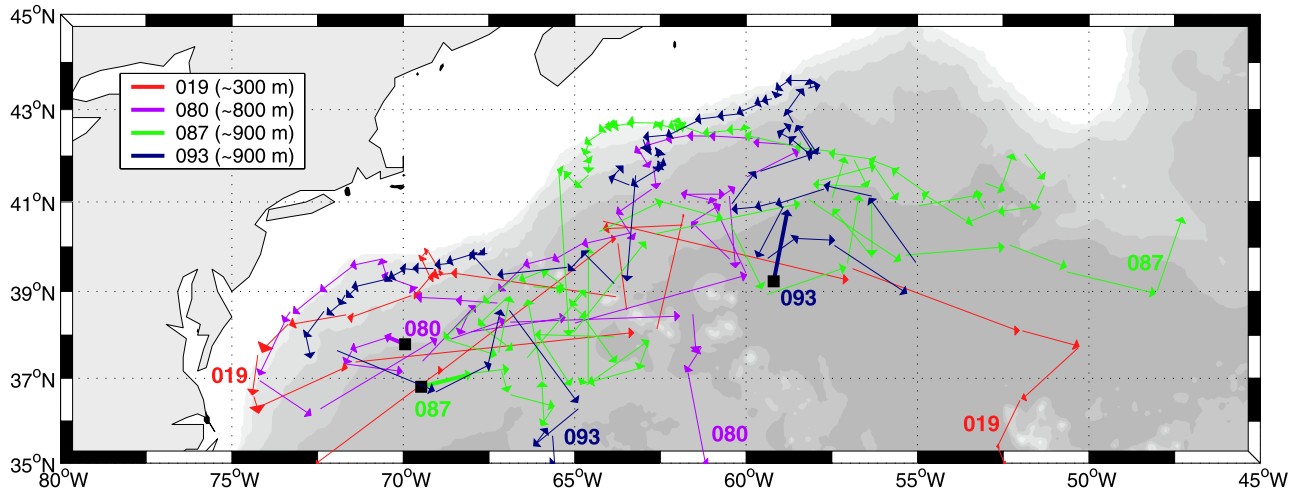
Figure 6. As in Figure 5, but for the trajectories of four floats that followed the northern recirculation gyre. Refer to the color bar in Figure 5 for the shading of the bathymetry.

[14] Float 004 continued to follow the counterclockwise route in the Iceland Basin and crossed the tip of the Reykjanes Ridge to return to the western basin and join the Irminger Current. Float 004 was drifting at about 450 m when it crossed the Reykjanes Ridge, where the bottom depth was almost 2000 m. Float 013 continued drifting northwestward near the Faroes-Shetland Channel to enter the Norwegian Basin. It reached to 72°N by following the
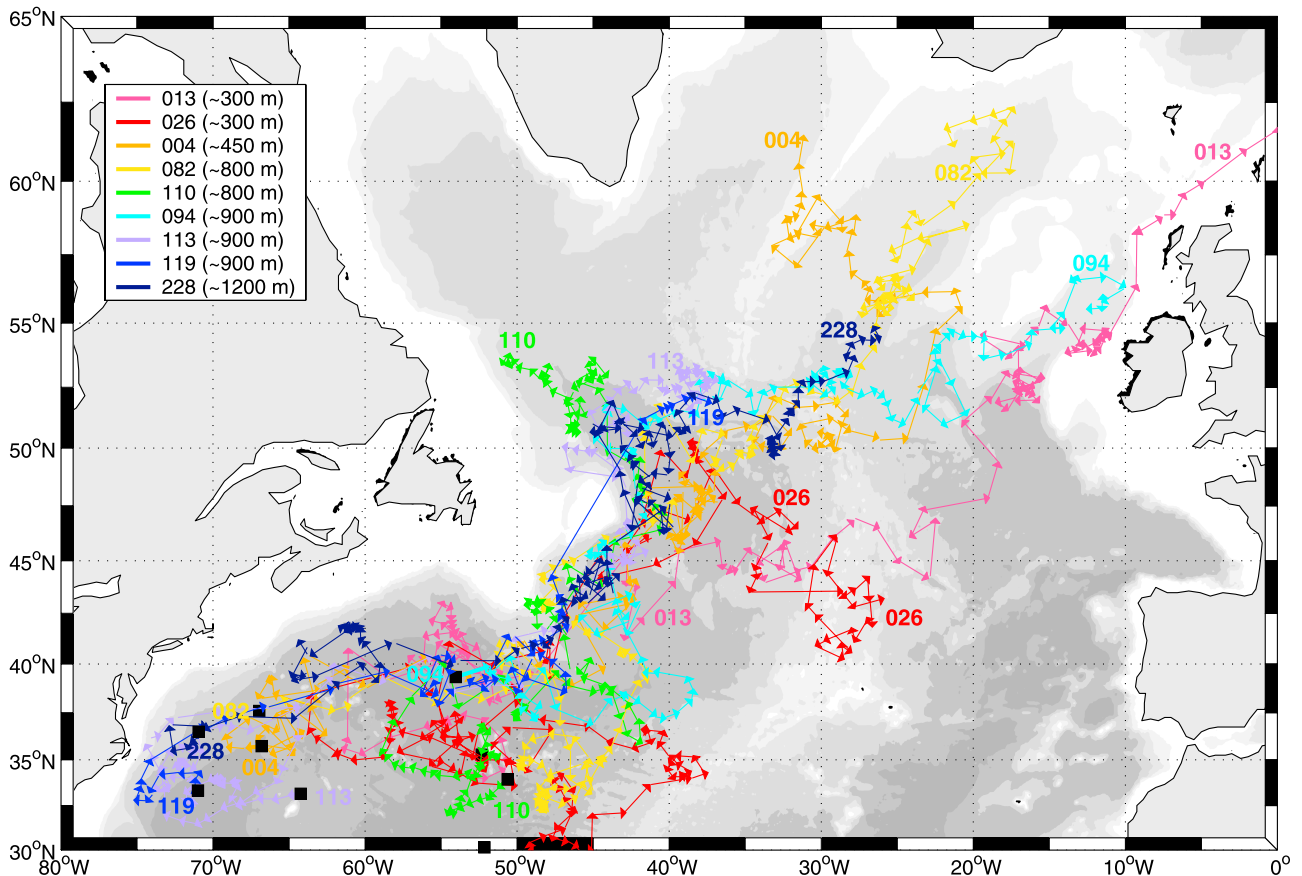
Figure 7. As in Figure 5, but for the trajectories of nine floats entered subpolar gyre. Refer to the color bar in Figure 5 for the shading of the bathymetry. The straight line over the Flemish Cap is not a real trajectory, but is due to the failure of Float 119 to surface for 106 days.
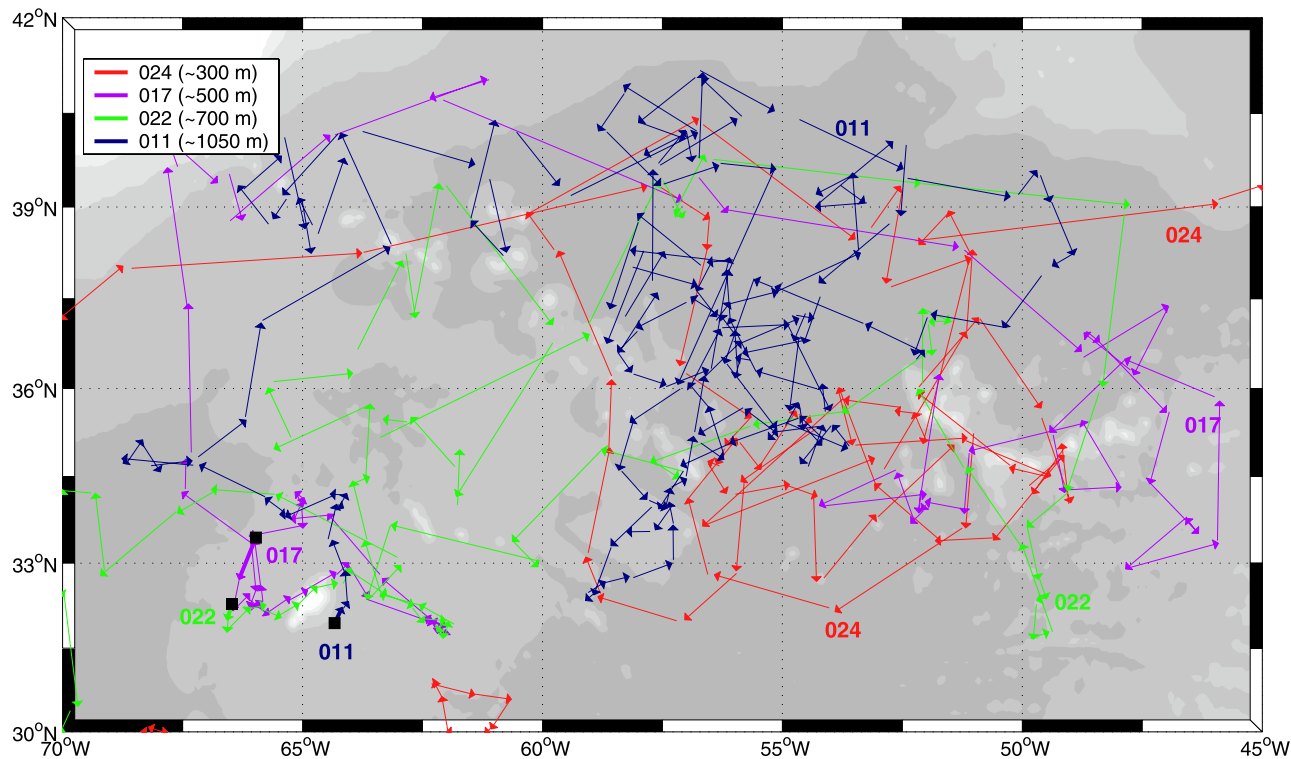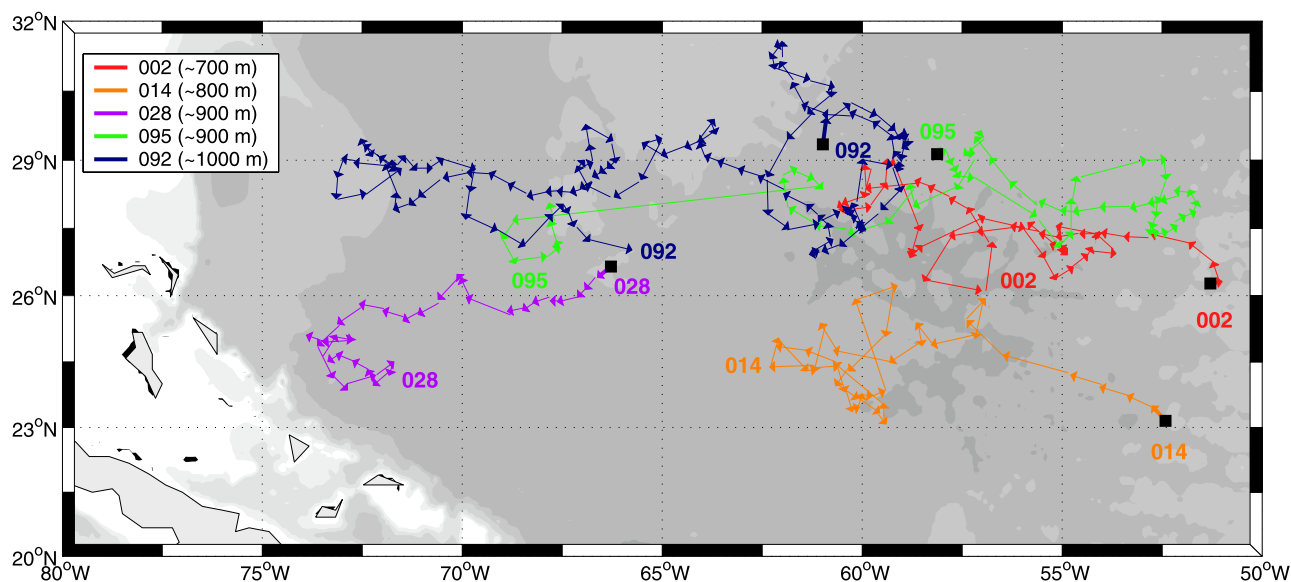
Figure 8. As in Figure 5, but for the trajectories of four selected floats that showed northward and eddy-like flow near Bermuda, the New England Seamounts, and Corner Rise. Refer to the color bar in Figure 5 for the shading of the bathymetry.

Norwegian Current along the northern continental slope of Norway [see *Poulain et al.*, 1996]. Note that the stream function map of *Bower et al.* [2002] also suggested that the floats crossing the Mid-Atlantic Ridge in the north through the Charlie-Gibbs Fracture Zone or the Faraday Fracture Zone have a highly likelihood of turning west into the Irminger Sea, while the floats crossing farther south have a

higher likelihood of continuing north towards the Nordic Seas.

3.4. New England Seamounts - Corner Rise - Bermuda

[15] Major topographic features of the western North Atlantic such as the New England Seamounts, the Corner Rise, Bermuda, and the Mid-Atlantic Ridge play a role as a

Figure 9. As in Figure 5, but for the trajectories of five selected floats that drifted in zonal flows in between 20°N and 32°N. The unusually long displacement of Float 095 between 61°W and 69°W is due to the loss of data for 150 days. Refer to the color bar in Figure 5 for the shading of the bathymetry.
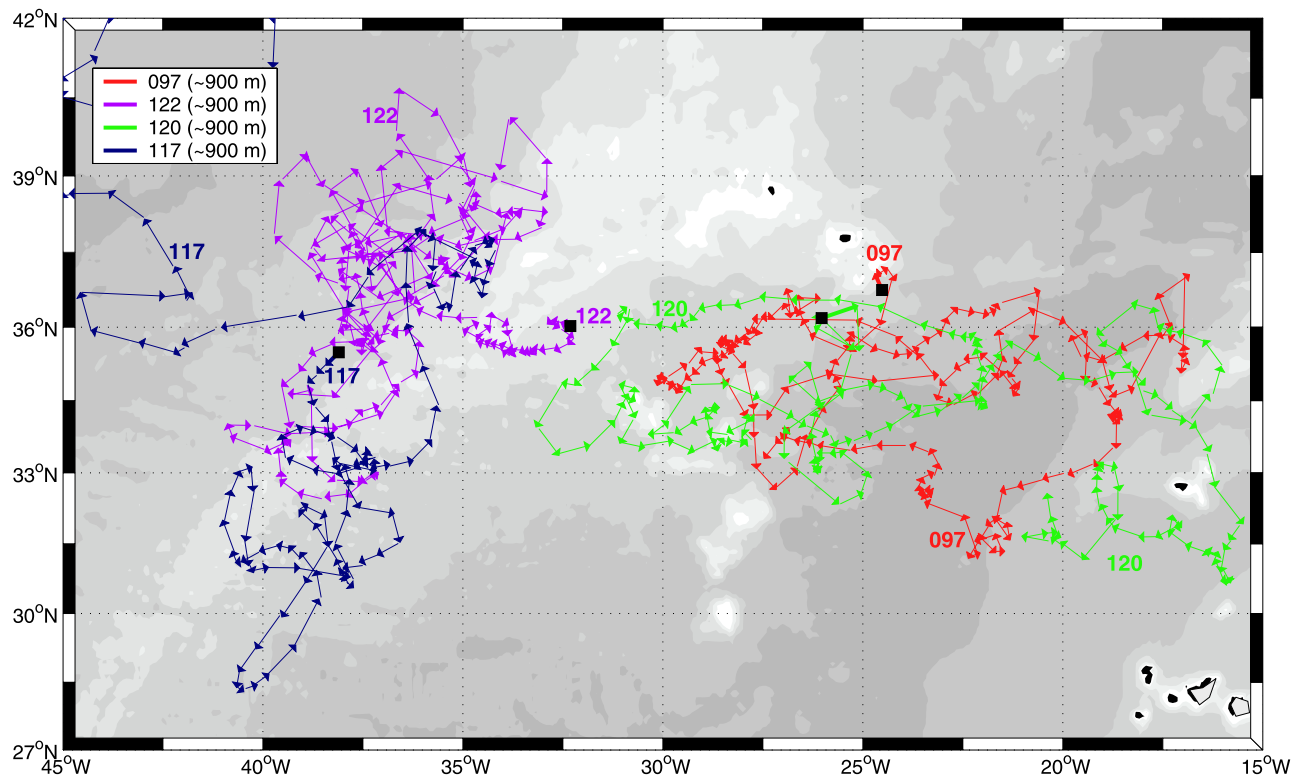
Figure 10. As in Figure 5, but for the trajectories of four floats in the either side of the Mid-Atlantic Ridge near the Azores front. Refer to the color bar in Figure 5 for the shading of the bathymetry.

barrier to eastward zonal flows. In addition to being blocked, many trajectories showed eddy-like behavior whenever the floats were near the topographic features and the overall displacements were often in the meridional direction rather than zonal (Figure 8). Blocked floats often traveled northward for extended periods before being entrained into the Gulf Stream, contrary to the expected south and southwestward flow of the anti-cyclonic gyre circulation. Float 011, which was deployed very close to Bermuda, drifted northward for the first 220 days at about 1050 m and was entrained into the Gulf Stream. Float 017, which was also deployed very close to the Bermuda, made a cyclonic loop with a radius of about 400 km for the first 280 days before traveling northward for the next 60 days to join the Gulf Stream at about 500 m. Float 022 drifted eastward from the deployment location west of Bermuda for the first 160 days of its life, then traveled northward for 90 days at about 700 m depth. Elsewhere, Float 024 showed similar steady northward drift for 50 days at about 300 m over the New England Seamounts. Other floats showed eddy-like motions superimposed on generally meridional displacements in these regions.

3.5. Zonal Flows in the Region South of 30°N

[16] *Rossby et al.* [1983] reported the existence of an eastward flow with the ensemble mean velocity of about 5 cm/s at 700 m depth in the region 20–30°N and east of 70°W. All six SOFAR floats they deployed in that area showed almost continuous eastward displacement from 30 days to 615 days, and none of them moved westward. Their observation was consistent with other observations

from current meter moorings [*Richman et al.*, 1977], and dynamic calculations using hydrographic data [*Reid*, 1978]. Our float observations suggest this mean eastward flow may not be ubiquitous or continuous in this region.

[17] Several of our floats showed net westward flow, with some extended period of eastward flow, in the same region (Figure 9). Float 014 traveled westward for the first 170 days along 24°N from 52°W before being trapped in an eddy-like motion around 60°W. Float 028 also drifted westward for the first 190 days along 26°N from 66°W to 73°W. Float 002 drifted westward for the first 25 cycles (~250 days) along the 27°N from 51°W to 61°W before turning toward the east and traveling eastward for the next 160 days back to 54°W. Float 095 traveled first 130 days eastward along 28°N from 58°W to 52°W and then drifted westward 260 days to get to 61°W. Other floats showed similar extended periods of zonal flow at comparable speeds in both directions; there was no apparent seasonality observed in these zonal flows.

3.6. Near the Mid-Atlantic Ridge

[18] The Azores Current flows eastward across the Mid Atlantic Ridge near 35°N near the surface [*Gould*, 1985]. Our floats in this region showed eddy-like motion primarily in meridional direction, along the flanks of the western side of the Mid Atlantic Ridge; float drifts in the eastern side of the ridge were mainly zonal along about 35°N (Figure 10). Three floats crossed the Mid-Atlantic Ridge at this latitude. Float 023 drifted eastward across the ridge at about 200 m depth (Figure 5). Float 122 was deployed on the eastern slope of the ridge and crossed the ridge several times while
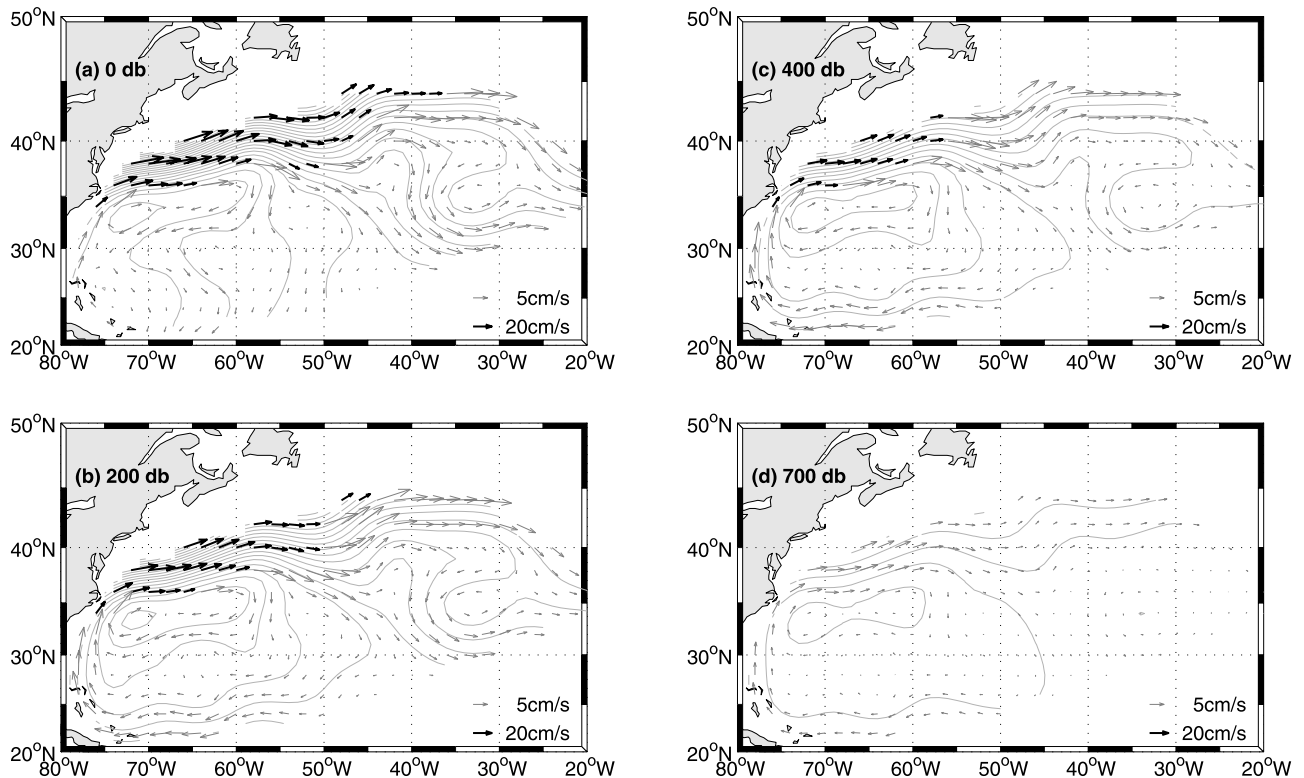
Figure 11. Geostrophic velocity (arrows) and the dynamic heights (contours) of the various depths relative to the 900 m level for January–March. Note that velocity has two different scales for the bold black arrows and the thin gray arrows. The contour interval for the dynamic height is 0.05 dynamic meter for all 4 levels.

mainly staying on the western slope of the ridge at about 900 m. Float 117 was deployed just west of the gap near 35°N, 38°W and traveled meridionally along the ridge and crossed the ridge several times for over 2 years before exiting the region by moving westward. Floats 097 and 120, deployed on the eastern flank of the Mid-Atlantic Ridge near 25°W, drifted almost zonally back and forth between 15°W and 32°W without crossing the ridge. Float 120 drifted eastward for 100 days, then began to move westward for 240 days along about 36°N at a depth of about 900 m. No apparent seasonality could be found related to these reversals of the zonal flow. *Spall et al.* [1993] reported similar low frequency zonal motion in the same region from 13 SOFAR floats at a slightly deeper depth (~1100 m). They suggested that baroclinic instability of the large-scale flow gives rise to low frequency zonal patterns similar to their observations.

## 4. Absolute Geostrophic Velocity Field

[19] Since profiling floats collect hydrographic observations and provide an estimation of the subsurface velocity simultaneously, an array of profiling floats can be used to estimate the absolute geostrophic velocity field. Using the North Atlantic ACCE floats, the relative geostrophic velocity field for upper 900 m was objectively mapped using hydrographic data collected from the profiling floats, and the reference velocity field at 900 m was calculated from the parking-depth float velocity estimates. These two fields were then combined to produce absolute geostrophic veloc-

ity estimates for the upper 900 m for each season of the annual cycle.

4.1. Relative Geostrophic Velocity

[20] The first step in the estimation of geostrophic velocity was to calculate dynamic height profiles from the sea surface to 900 m depth for each observation and produce objectively mapped relative geostrophic velocities for the upper 900 m. This was complicated by the fact that for 90% of the profiles, only temperature data were collected (i.e., salinity was not measured). Typically, about 2100 temperature-only profiles and 240 CTD profiles were available for each mean seasonal field (Figure 3). To overcome the lack of salinity observations, salinity was estimated for the temperature-only profiles using the temperature-salinity (*T-S*) relation from the Hydrobase2 climatology [*Lozier et al.*, 1995] (see Appendix A).

[21] Another complication was that not all the profiles extended from the sea surface to 1000 m, mainly due to the gradual shoaling of the parking depth on many floats (Figure 4). The number of observations at both the shallowest and the deepest parking depth levels were smaller than those of the mid-depth levels because of this problem (Figure B1). Since the objective mapping was performed independently for each standard depth, levels with an insufficient number of observations (a few levels near the top and the bottom of the entire range of parking depths) tended to produce fields that were less reliable and inconsistent with the other levels. As a result, an additional vertical constraint was introduced using the extrapolation
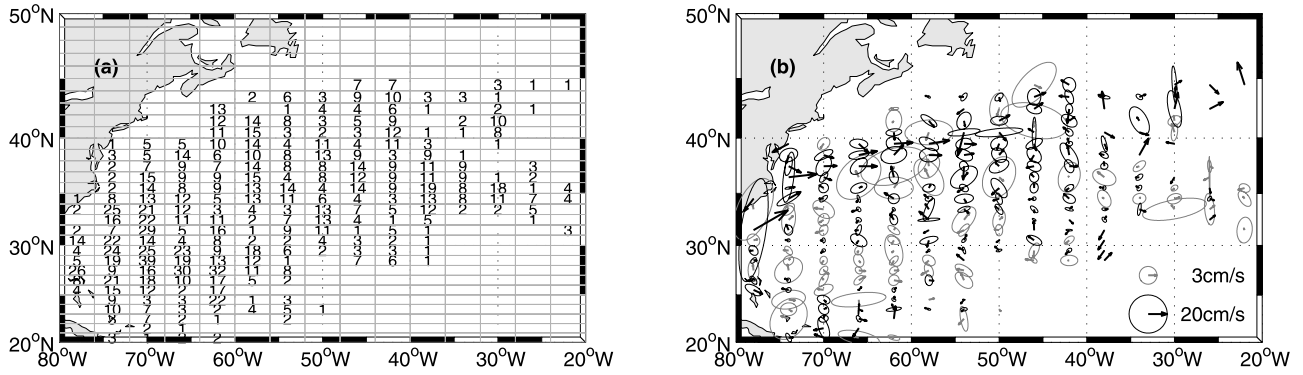
Figure 12. Data used for the reference velocity mapping at 900 m for January–March. (a) Number of parking-depth velocity observations for each 4° longitude × 1° latitude bin. (b) Bin-averaged velocity and standard error ellipses. Note that velocity arrows and standard error ellipses have two different scales.

of the dynamic height profiles to improve the vertical coherence (discussed in detail in Appendix B).

[22] Using the estimated dynamic height profiles, the geostrophic velocity and the streamfunction were objectively mapped for 21 standard depths from the sea surface to 900 m. A Poisson-type covariance function with a 500 km decorrelation length scale was used and a mapping error of 10% was allowed for the objective mapping [*Bretherton et al.*, 1976]. A second order polynomial of the form $F(x, y) = a_0 + a_1 x + a_2 y + a_3 x^2 + a_4 y^2$ was assumed for the large-scale background field [*Le Traon*, 1990]. The local nondivergent

relation of the horizontal velocity was built in the objective mapping of the streamfunction by calculating the velocity simultaneously with the streamfunction using derivatives of the covariance matrix [*Bretherton et al.*, 1976; *McWilliams*, 1976].

[23] As shown for the winter fields (Figure 11), the relative velocity fields all contained a wide Gulf Stream and a smooth southern recirculation gyre. The Gulf Stream was wider than reality mainly because of the spatial smoothing introduced by the objective mapping procedure. The mapping did not reproduce the eddy-like topographic
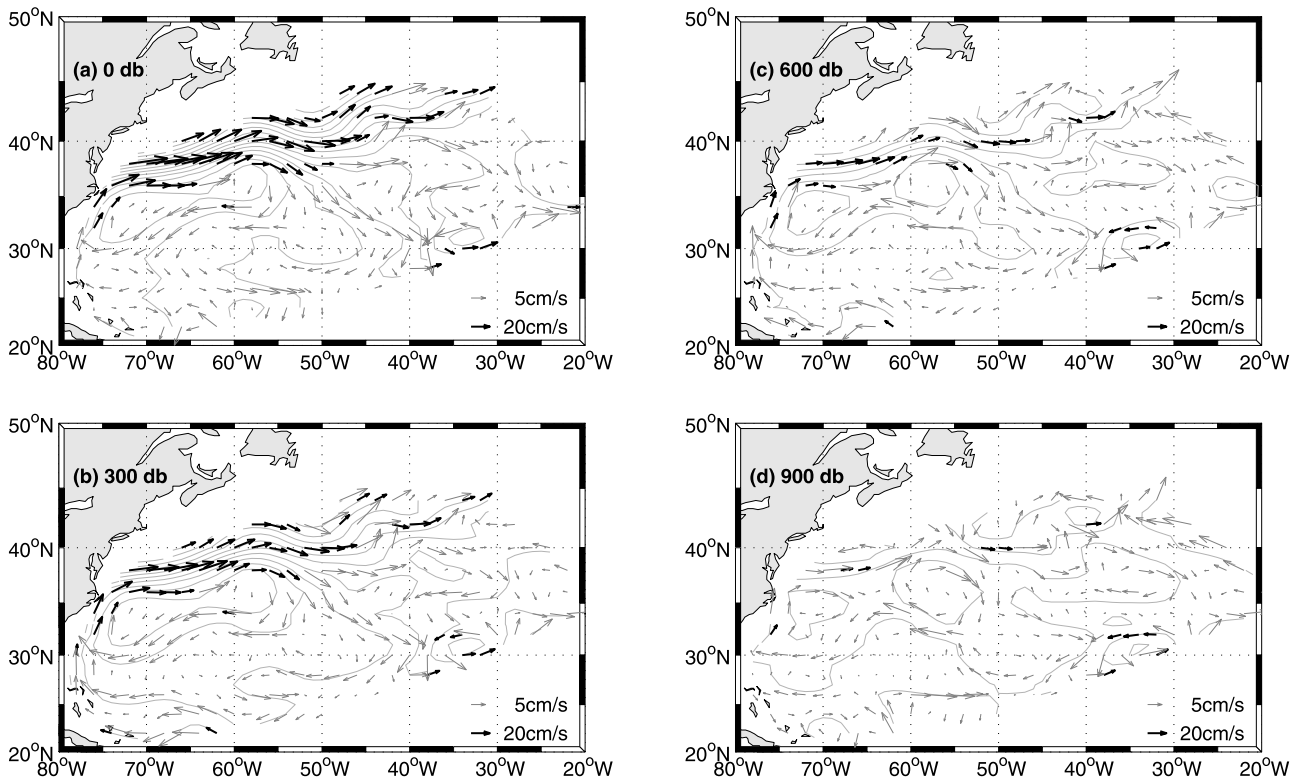
Figure 13. Absolute geostrophic velocity (arrows) and the absolute pressure (contours) of the various levels for January–March. Note that velocity has two different scales for the bold black arrows and the thin gray arrows. The contour interval for the pressure is 0.10 dynamic meter for all 4 levels. Figure 13d is also the reference velocity field since the relative velocity is zero at 900 db.
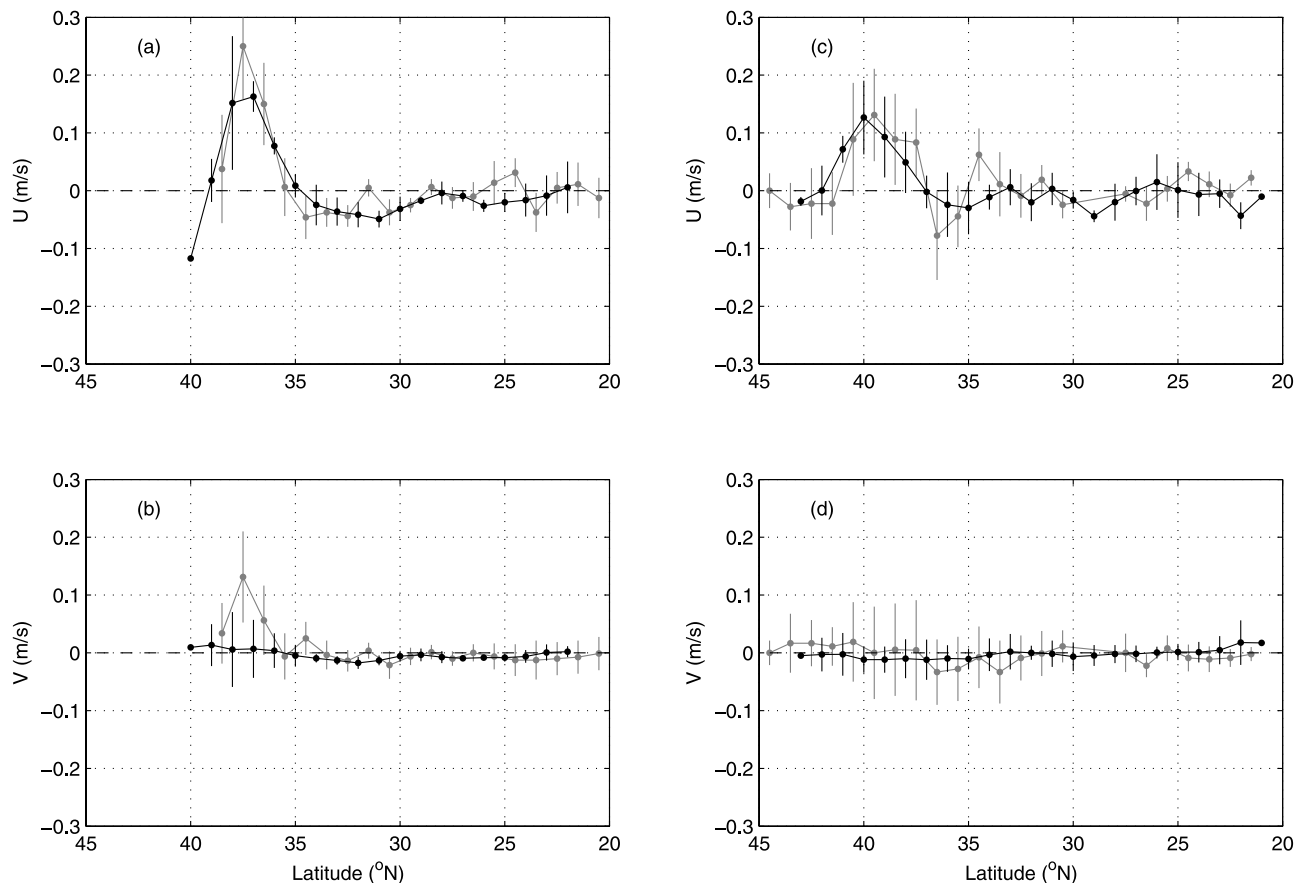
Figure 14. Mean velocity profiles at 700 m along the meridional sections at 70°W and 55°W. (a, c) Zonal velocity at each latitude. (b, d) Meridional velocity at each latitude. Black lines are the average of absolute geostrophic velocity of four seasons with the error bar of the one standard deviation. The gray lines are corresponding velocity profiles from *Owens* [1991] (see his Figures 25–26, 28–29 for the detail).

influence in the southern recirculation gyre that was seen in the float trajectories. The only trace of the topographic influence was the isolated anticyclonic flow near 35°N, 60°W seen in summer and autumn maps at some intermediate depths (not shown here). The surface relative geostrophic flow map showed a C-shaped feature of the dynamic height contour in the southwestern quadrant of the region, apparently similar to that described in the surface dynamic height field relative to 1000 db by *Reid* [1978]. The Gulf Stream showed a maximum velocity of 30 cm/s at the surface and of 5 cm/s at 700 m depth, generally smaller than observed but consistent with a Gulf Stream that is too wide (and hence too slow). The remainder of the southern recirculation gyre away from the Gulf Stream showed typical speeds in the range of 3 cm/s.

4.2. Reference Velocity at 900 m

[24] Parking-depth float velocity between two consecutive ascents was estimated based on the location and time information from the last satellite fix during the preceding profile and the first fix during the following profile. No attempt was made to extrapolate the time/location to the exact points of surfacing and diving [*Davis et al.*, 1992]. *Park et al.* [2005] suggested that the error in the parking-depth velocity due to no extrapolation would be on the order

of 0.1 cm/s, which is negligible for the purpose of our study. Since the parking depth gradually shoaled over the lives of some floats, the observed parking depth velocities had to be brought to a common depth in order to produce a consistent reference velocity field. Thus, the parking depth velocity was projected to a depth of 900 m (actually 900 decibars) for each profile by using the geostrophic shear inferred from the dynamic height calculation. For consistency, the geostrophic shear produced from the relative velocity calculation was used for carrying out this projection, rather than using climatology. A bin averaging procedure was then carried out for each 4° longitude by 1° latitude bin in order to lower the noise level and enhance the statistical significance of the resulting velocity. The bin-averaged 900 m velocity was objectively mapped to fill the missing bins. Decorrelation lengths of 500 km in zonal direction and 200 km in meridional direction were used for the objective mapping. The mapping allowed a 10% of local random error, and the same second order background large-scale field was assumed as for the relative velocity mapping. The number of observations for each bin for the winter mapping (similar to the numbers for the other seasons) is given in the Figure 12a. Most of the bins contained between 8 and 20 observations, with slightly more data in the region west of 55°W. Bins in the southwestern quadrant of the gyre had the
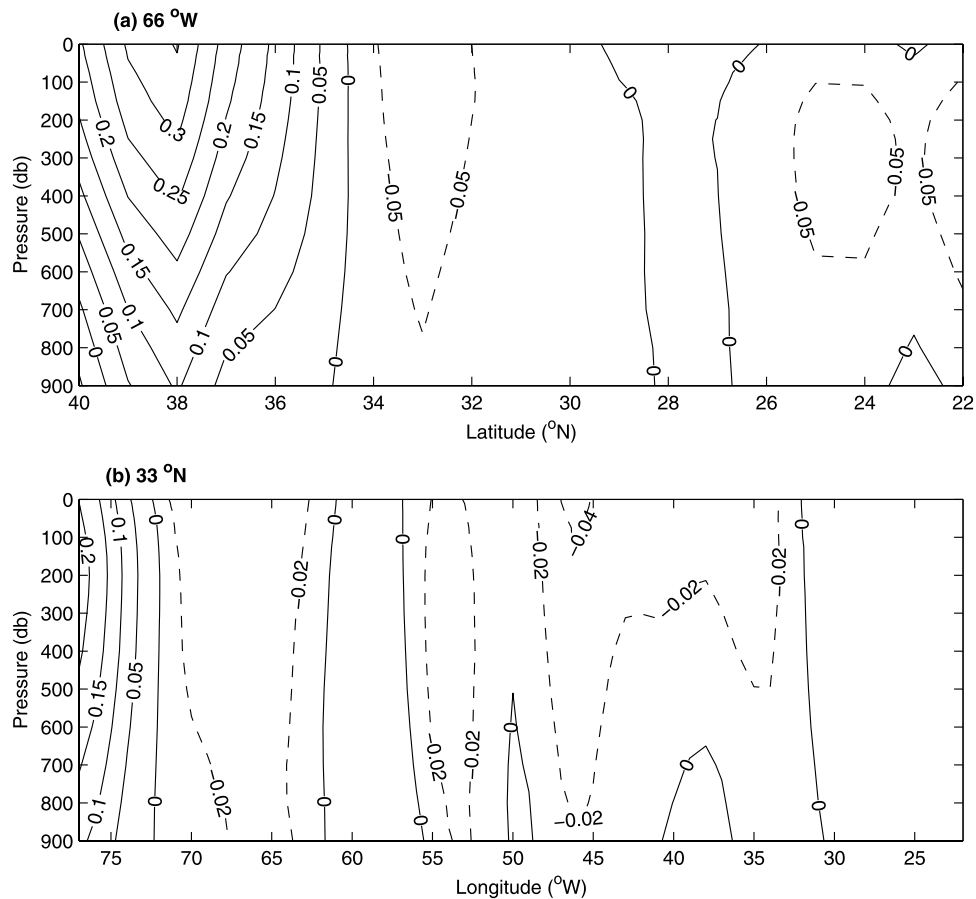
Figure 15. Velocity sections across the gyre. (a) Zonal velocity section along 66°W. (b) Meridional velocity section along 33°N. Units for the contour labels are m/s. Positive and zero contours are in solid curves, and negative contours are in dashed curves.

maximum concentration of observations, up to 39. The bin averaged velocity and the associated standard error ellipses for winter are plotted in Figure 12b. The standard error in each bin average is defined as the root-mean-square variance divided by the square root of the number of independent observations, following *Owens* [1991]. The ellipse was calculated using the method of *Freeland et al.* [1975]. The bin averaged absolute velocity showed the Gulf Stream and the recirculation gyre somewhat less clearly than the relative velocity fields (Figure 11). Error ellipses were often bigger and oriented along the northwest-southeast direction near the major topographic features, which reflected the eddy-like nature of the already described in the trajectories from these regions.

[25] The reference velocity maps in general showed more spatial structure than the relative velocity maps. These features appeared to be mainly related to the topography. The reference velocity field for winter showed the isolated anti-cyclonic gyre and associated meridional flow around 60°W bisecting the southern recirculation gyre (Figure 13d). Meridional flows and double gyre features also appeared in spring and summer maps (not shown). These features originated from the meridionally oriented eddy-like motions of the float trajectories described in the previous section and could not be smoothed out by the choice of a larger decorrelation length scale for the objective mapping. The

900 m reference velocity in the Gulf Stream extension was typically about 10 cm/s and about 5 cm/s in the recirculation region.

4.3. Absolute Geostrophic Velocity

[26] The total velocity fields (the absolute geostrophic velocity fields for the upper 900 m) were produced by adding the relative fields and the reference field of the corresponding season. Figure 13 shows the winter absolute geostrophic velocity fields at selected depths. Not surprisingly, the upper levels tend to show more of the features from the relative velocity fields and the lower levels tend to represent more of the reference velocity field. The Gulf Stream has a velocity of about 35 cm/s at the surface and about 15 cm/s at 900 m depth in these maps, which is considerably smaller than directly observed values [*Rossby and Gottlieb*, 1998]. The poor representation of the strong boundary current and its extension near the surface was unavoidable due to the two-fold smoothing operation, the bin averaging and the objective mapping. On the other hand, the maps of the ocean interior, away from the boundary currents, seem very reasonable and consistent with the previous direct observations (Figure 14).

[27] Velocities at 700 m along two sections, 70°W and 55°W, were compared with the previous direct observations of *Owens* [1991] (Figure 14). The velocity sections from
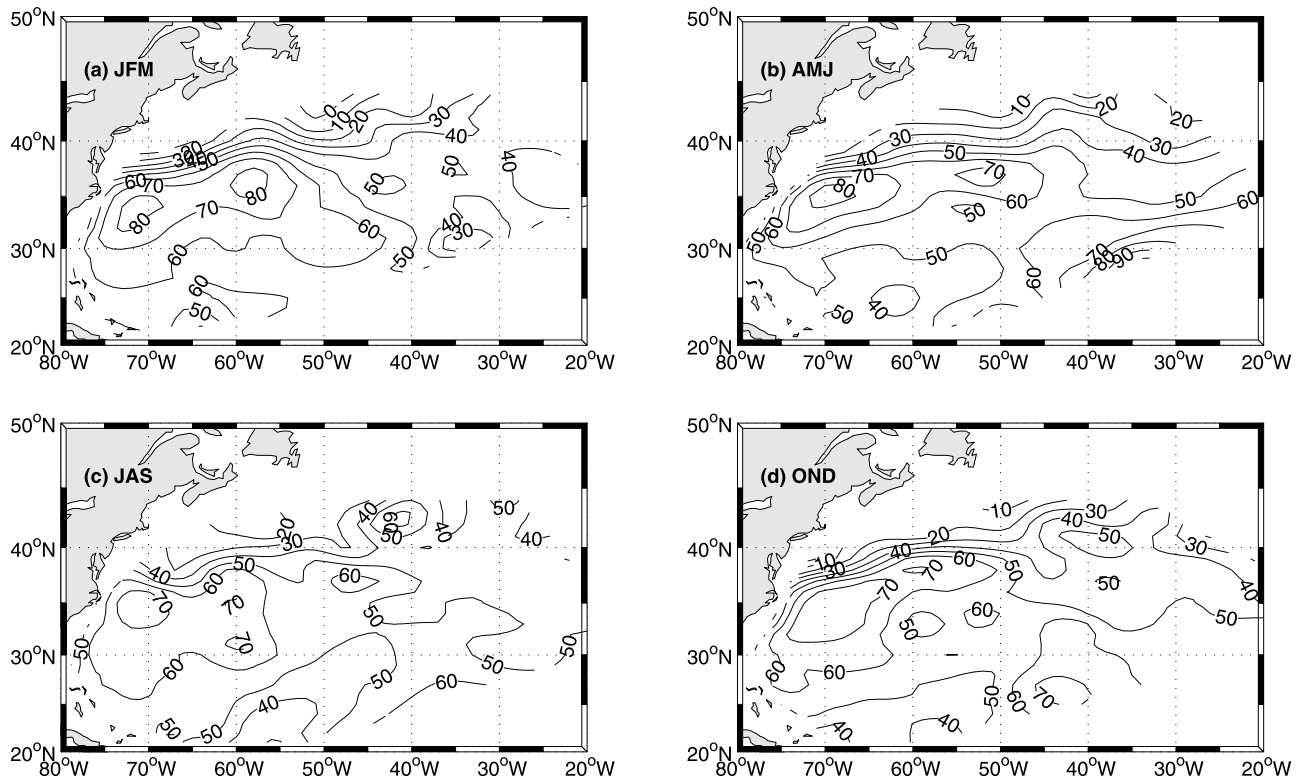
Figure 16. Volume transport streamfunction for the upper 900 m of (a) January–March, (b) April–June, (c) July–September, and (d) October–December. Units for the contour labels are Sv($=10^6$ m^3/s).

Owens [1991] were based on a 5° longitude by 1° latitude bin average using two decades of SOFAR float observations beginning in 1972. The two velocity estimates were remarkably consistent at all latitudes in both the zonal and the meridional directions. The one exception was the relatively large meridional velocity at 70°W near 38°N (Figure 14b), where the spatial coverage of the ACCE observations was relatively poor. This relatively stationary feature of the Gulf Stream system between two periods separated by more than a decade was consistent with the result from 10 years of ADCP measurements from the Oleander Project [*Rossby and Gottlieb*, 1998; *Rossby and Zhang*, 2001].

[28] Two gyre cross-sections are presented in Figure 15 in order to allow a more detailed examination of the vertical structure of the gyre. The meridional section of the zonal velocity along 66°W clearly shows the well-known baroclinic structure of the Gulf Stream centered at 38°N, with the maximum velocity over 35 cm/s at the surface (Figure 15a). The tilt of the maximum velocity axis was not reproduced in this map due to insufficient spatial resolution. The southwestward recirculation was broadly distributed to the south of the Gulf Stream extension with a narrow band of weak return flow centered around 25°N and a small region of apparently weak eastward flow around 27°N. The westward return flow had the mean velocity of about 4 cm/s with the maximum velocity of about 9 cm/s; the vertical structure of the return flow was relatively barotropic compared to the eastward flowing Gulf Stream. The float-derived velocity field along this section appears to agree well with the *Joyce et al.* [2001] synoptic LADCP section along the same longitude made in 1997; even the

narrow band of apparent eastward flow around 27°N could be found in both sections.

[29] Zonal sections of float-derived meridional velocity along the 33°N (Figure 15b) show a portion of the Gulf Stream near 75°W at the western end of the section. This part of the Gulf Stream, upstream of the separation point near the Cape Hatteras, seems to have smaller vertical shear compared to the meandering eastward jet at 38°N shown in Figure 15a. A southward return flow was distributed broadly from 72°W to almost 30°W, with a mean velocity of about 2 cm/s. The meridional flow showed reversals near the major topographic features, especially east of Bermuda around 60°W.

5. Volume Transport

[30] Figure 16 shows the volume transport stream function for the upper 900 m calculated from the float-derived absolute velocity field. Volume transport was about 40–70 Sv in the Gulf Stream and about 20–30 Sv in the southwestward and westward return flow. The volume transport of the Gulf Stream system is clearly a minimum in summer months (July–September) and maximum in winter, but the winter values are just slightly greater than those of spring and autumn. The baroclinic volume transport stream function, defined to be the integral of relative geostrophic velocity with the level of no motion at 900 decibars [*Hogg*, 1992], is presented in Figure 17. Seasonal differences were much smaller in the baroclinic transport than the barotropic transport, but a minimum was still found in summer months. The baroclinic transport was
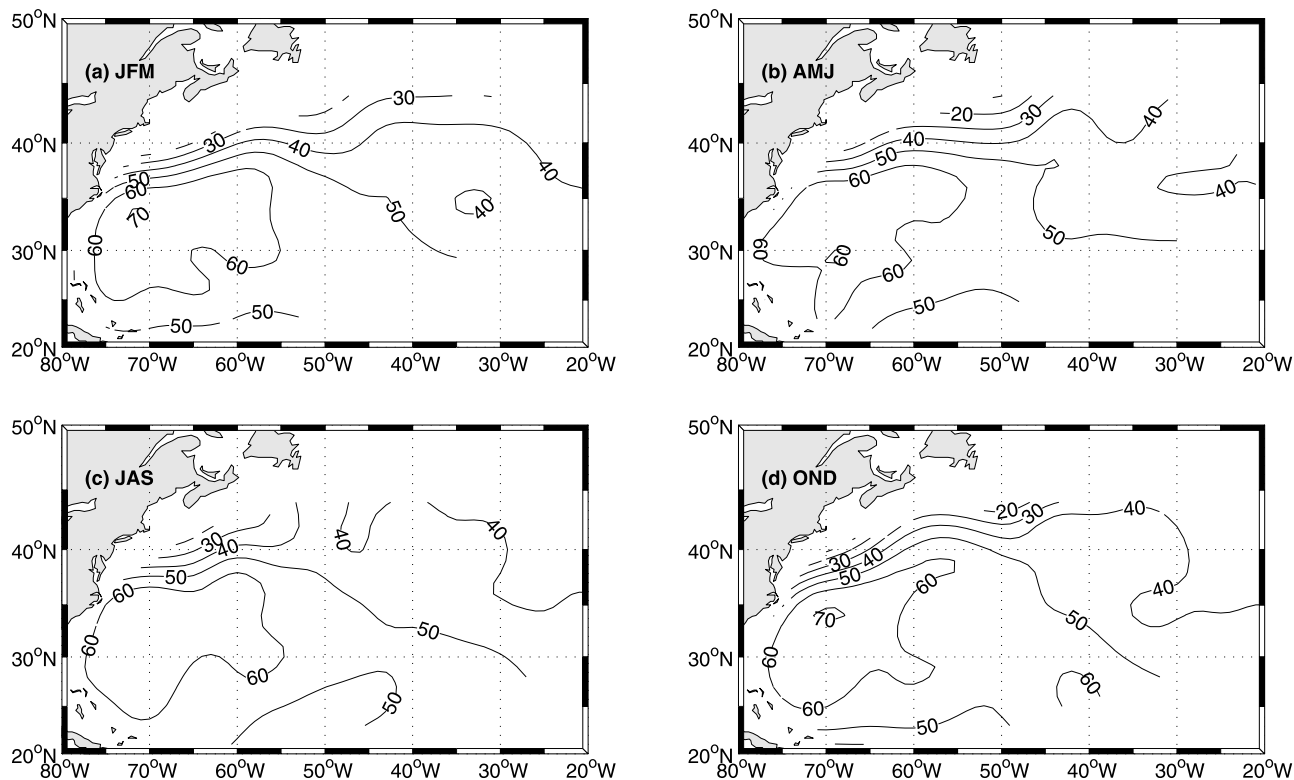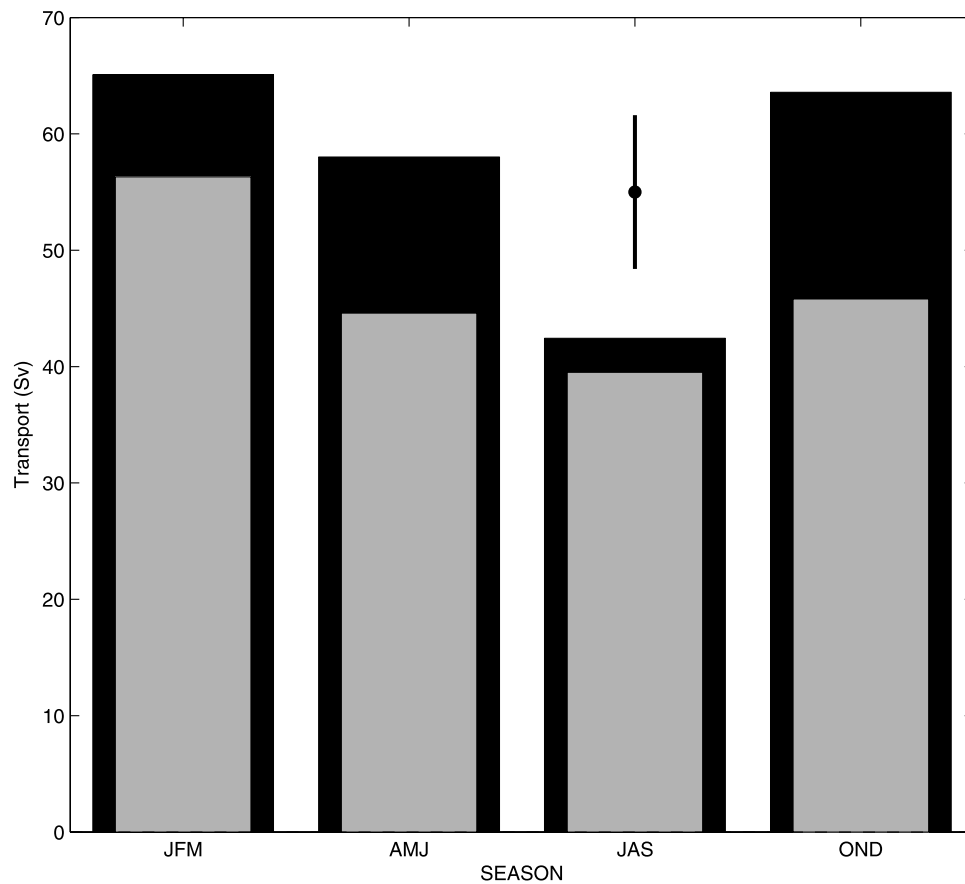
Figure 17. Baroclinic volume transport stream function for the upper 900 m of (a) January–March, (b) April–June, (c) July–September, and (d) October–December. Units for the contour labels are Sv(=10^6 m^3/s).

found to be about 40–50 Sv in the Gulf Stream and 10–20 Sv in the recirculation gyre.

[31] Since the velocity field and thus the volume transport stream function failed to cover the full extent of the Gulf Stream in the meridional direction, a second order polynomial fit to the meridional profile of depth-integrated velocity was carried out in order to include the missing part at the northern end of the section [*Halkin and Rossby*, 1985]; results of this calculation are shown in Figure 18. For the all sections except for the July–September, one additional degree latitude at the northern end of the sections had to be extrapolated to cover the full extent of the Gulf Stream (the July–September section already covered the full extent of the Gulf Stream). Using this method, the Gulf Stream volume transport at 64°W was found to be 65 Sv in winter and 42 Sv in summer. The baroclinic volume transport in the same section showed a similar seasonal cycle, with 70% of the amplitude of the total transport. Note that only the difference between winter and summer transports was large enough to be meaningful relative to the estimated error (see Appendix C for the detail of the error estimation). This winter maximum/summer minimum in the Gulf Stream and the southern recirculation gyre transports are in-phase with the atmospheric wind and heat flux forcing. The first empirical orthogonal functions (EOFs) of wind stress and wind stress curl from NCEP-NCAR reanalysis [*Kalnay et al.*, 1996], explained about 80% and 63% of the total variance, respectively. Both the leading EOFs of wind stress and wind stress curl showed a maximum in January and a minimum in July. Also, the first EOF of the net surface heat

flux, which explains 98% of the total variance, has a maximum in January and minimum in June and July. Thus, it appears that the subtropical gyre of the North Atlantic is responding nearly in phase to its primary driving mechanisms.

[32] The transport of the Gulf Stream and its seasonal cycle has been a subject of long interest and debate (see the summary in Table 2). *Worthington* [1976] estimated the transport near 70°W based on the geostrophic velocity relative to 2000 db from 32 hydrographic sections taken between Long Island and Bermuda from 1932 to 1968. He found that the maximum transport of about 85 Sv is in January–April, with a minimum transport of about 70 Sv around October–December. *Watts* [1983] arrived at the same conclusion using XBT data collected from 1970–1973. However, *Sato and Rossby* [1995] used the same method as *Worthington* [1976] with a larger data set and they concluded the transport was maximum in June and minimum in December; their annual cycle, however, accounted for only about 10% of the total variance and was almost completely out of phase with our estimation and also with *Worthington*'s [1976] result. They also presented transport relative to the 300 db, which showed the minimum in April and the maximum in October. *Halkin and Rossby* [1985] reported Gulf Stream transport around 73°W from an extensive survey during September 1980–May 1983 using the Pegasus, a free-falling velocity profiler. Their estimation of the upper 2000 m total transport was 87.8 Sv ± 17.3 Sv. Their transport showed a large scatter with a maximum in March and a second-

Figure 18. Seasonal volume transport of the Gulf Stream for the 900 m level at 64°W. Black bars are for the total transport, and the gray bars are for the baroclinic transport. See Appendix C for the method of error estimation.

ary maximum in September, and minimum values were found in May and August. *Rossby and Gottlieb* [1998] showed that transport per unit depth at 52 m depth from a repeated ADCP observation between Port Elizabeth, New Jersey and Bermuda had maximum in fall and minimum in spring. *Fu et al.* [1987] analyzed 3.5 years of satellite altimeter data between April 1975–November 1978 and concluded that the sea level difference across the Gulf Stream was a maximum in April and minimum in December. *Kelly et al.* [1999] also used altimeter

Table 2. Summary for the Seasonal Cycle of the Gulf Stream Transport From Previous Studies

Reference	Maximum Transport	Minimum Transport	Variance Explained by the Annual Cycle	Methods	Study Periods	Location
Worthington [1976]	Jan–Apr	Oct–Dec		Baroclinic transport relative to 2000 db	1932–1968	~70°W
Watts [1983]	Jan–Apr	Oct–Dec		Cross-Stream temperature gradient	1970–1973	~70°W
Sato and Rossby [1995]	Jun	Dec	10%	Baroclinic transport relative to 2000 db	1932–1988	~70°W
	Apr	Oct	5%	Baroclinic transport relative to 300 db		
Halkin and Rossby [1985]	Mar	May, Aug	Statistically not significant	Total transport above 2000 m from Pegasus profiler	1980–1983	~73°W
Rossby and Gottlieb [1998]	Sep	Mar		Transport per unit depth at 52 m from ADCP	1992–1997	~70°W
Fu et al. [1987]	Apr	Dec		EOF of cross-Stream SSH gradient from satellite altimeter	1975–1978	70–75°W
Kelly et al. [1999]	Oct	Apr	7–40%	Cross-Stream SSH gradient from satellite altimeter	1992–1994	64–73°W
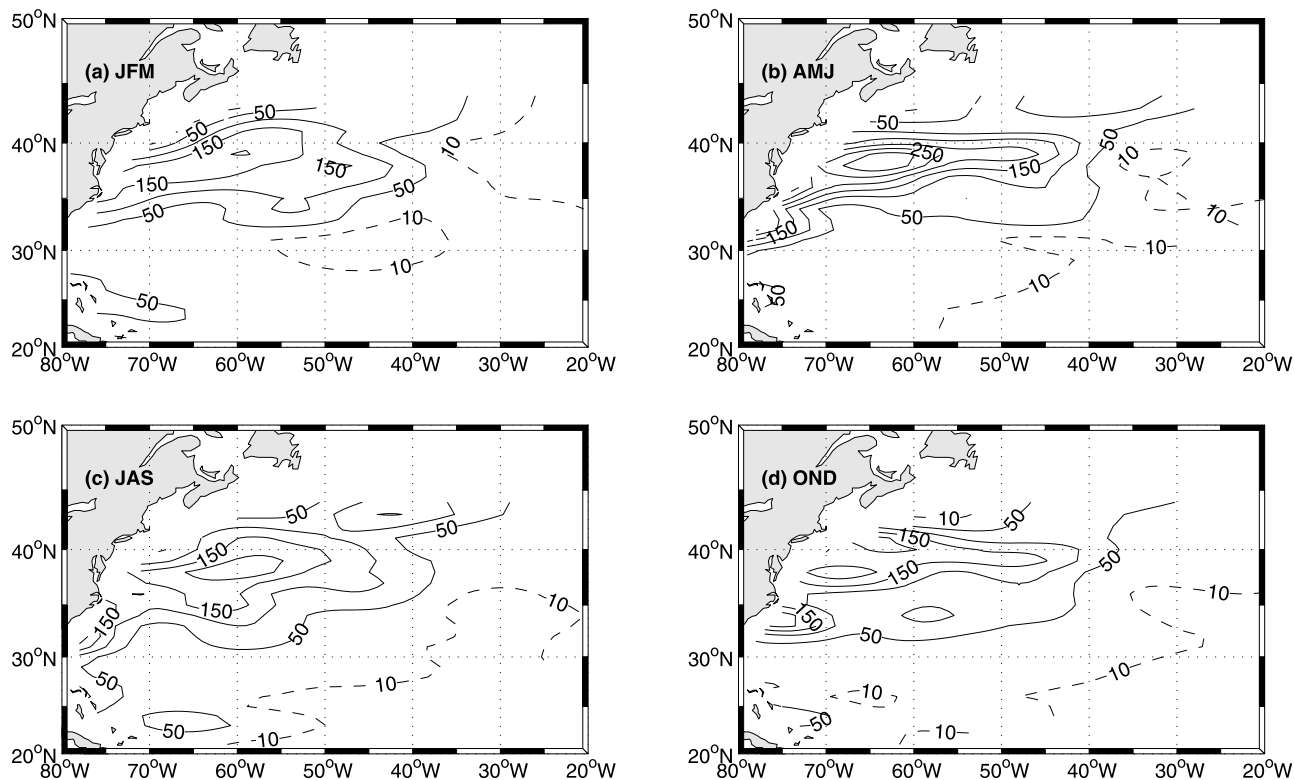
Figure 19. Eddy kinetic energy at 900 m for (a) January–March, (b) April–June, (c) July–September, and (d) October–December. Units for the contour labels are 10^{-4} m^2/s^2.

observations during November 1986–April 1989 and October 1992–November 1994, but concluded that the sea surface height difference across the Gulf Stream was a maximum in fall and minimum in spring.

[33] The diverging results on the seasonal cycle of the Gulf Stream transport perhaps suggest that the Gulf Stream transport does not have a significant seasonal cycle compared to the variability in the other frequency bands. The low percentages of the total variance explained by the annual harmonic in most of these studies add some ground to this speculation. *Lee and Cornillon* [1995] reported that the AVHRR-derived meandering intensity of the Gulf Stream for the period April 1982 through December 1989 displayed a 9-month dominant periodicity, while its annual variation was weak. Unfortunately, our data limit our analysis to the seasonal climatology, and observations with a better spatial resolution and longer duration will be required to resolve this issue.

## 6. Eddy Kinetic Energy and Diffusivity

[34] The eddy kinetic energy (EKE) and diffusivity in the zonal and meridional directions at 900 m for each season were estimated from the parking-depth velocity observations. Parking-depth velocities were projected to 900 m using the geostrophic shear and grouped into 4° longitude by 1° latitude bins, as already described for the calculation of the reference velocity fields. The perturbation velocities, i.e. u' and v', were then calculated relative to the mean velocities of each bin. The parameterization of *Davis* [1987]

was used for the diffusivities k_x and k_y in zonal and meridional direction,

$$k_x = T_L \langle u'^2 \rangle, k_y = T_L \langle v'^2 \rangle$$

where T_L is the Lagrangian integral timescale, and the brackets denote the ensemble average for each bin. A constant Lagrangian integral timescale of 6 days was used based on the previous Lagrangian calculation from this region [*Rossby et al.*, 1983; *Boning*, 1988; *Lumkin et al.*, 2002].

[35] The EKE at 900 m showed a concentrated maximum value along the Gulf Stream region (Figure 19), with values greater than 0.015 m^2/s^2 throughout the year. The maximum value was found in spring months (April–June), with the peak greater than 0.030 m^2/s^2; the minimum was found in winter months. Interior values are less than 0.005 m^2/s^2 and have relatively small seasonal variability. These results can be compared to the estimates of *Ducet et al.* [2000], who showed that EKE derived from satellite altimeter data had a maximum in spring in the vicinity of the Gulf Stream and in summer in the recirculation gyre. However, their annual harmonics explained less than 20% of the total EKE variance in these regions. *Stammer and Wunsch* [1999] also presented seasonal maps of EKE from TOPEX/POSEIDON altimeter showing a clear minimum in December–February in the western subtropical North Atlantic including the Gulf Stream region and slight maximum in March–May. *Richardson* [1983] used surface drifters to calculate monthly values of EKE, which showed a maximum in the
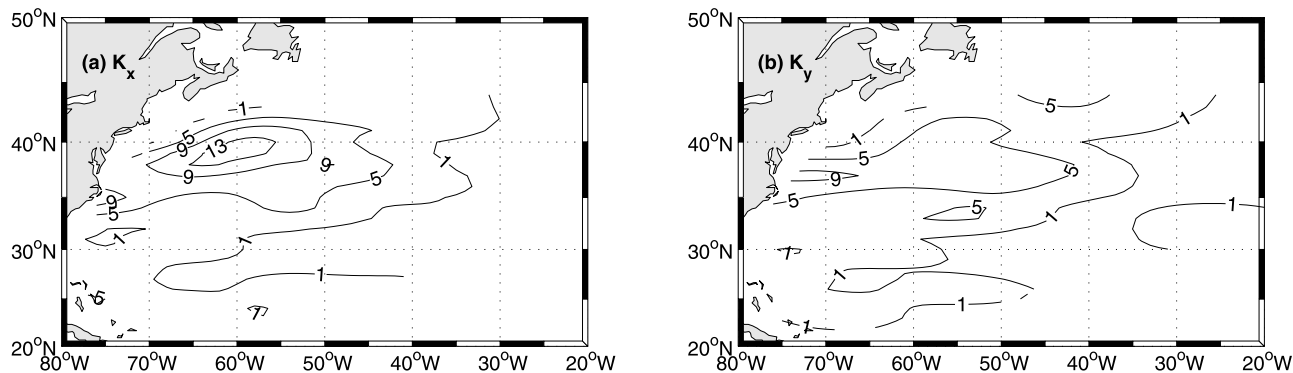
Figure 20. (a) Zonal diffusivity and (b) meridional diffusivity at 900 m for January–March. Units for the contour labels are 10^3 m^2/s.

April–June period and minimum in November–February in the vicinity of the Gulf Stream. The spring maximum of the EKE, from our analysis and also from the previous studies, is consistent with our winter maximum in the Gulf Stream transport, if baroclinic instability is the main source of the EKE. The spatial structure of EKE at 900 m is similar to that at the sea surface, but the values at 900 m are only about 10% of the EKE at the surface [*Ducet et al.*, 2000; *Frantantoni*, 2001; *Reverdin et al.*, 2003]. The float-derived values are also comparable with previous estimates in similar depth ranges [*Richardson*, 1985; *Schmitz and Holland*, 1986].

[36] Diffusivity estimated from the floats showed similar spatial structure and seasonal cycles to those of EKE (Figure 20). The zonal and meridional diffusivities were comparable except for the core of the Gulf Stream region, where both estimates showed a maximum and the zonal diffusivity was about 50% greater. Within the maximum core, meridional diffusivity reached 0.01 m^2/s in spring months, while the maximum zonal diffusivity were greater than 0.02 m^2/s, also in spring. Diffusivity in the interior region was less than 0.005 m^2/s and had no significant seasonal differences. These estimates are comparable to previous estimates based on both float observations and high-resolution numerical models [*Rossby et al.*, 1983; *Boning*, 1988; *Lumkin et al.*, 2002].

7. Summary

[37] The general circulation of the western subtropical North Atlantic was described in quasi-Lagrangian and Eulerian perspectives using observations from the 71 ACCE/WOCE profiling floats during the July 1997–December 2002 time period. The major conclusions inferred from the profiling float data set can be summarized as follows:

[38] 1. Both the Gulf Stream and the southern recirculation gyre showed strong depth-dependence and topographic influences. At greater depths the gyre appeared to be smaller and was more confined to the northwestern corner of the Sargasso Sea. The zonal extent of the gyre was apparently limited by major topographic features, such as the New England Seamounts and the Mid Atlantic Ridge.

[39] 2. There was no preferred location for entrainment from the interior of the recirculation gyre into the Gulf Stream; entrainment appeared to occur continuously from the Florida Straits to Cape Hatteras, even continuing in some cases downstream. Some floats even showed extended northward drift from the region near Bermuda and the New England Seamounts to the Gulf Stream.

[40] 3. Alternating zonal flows were observed near 35°N, east of Mid-Atlantic Ridge and near 28°N in the subtropical convergence zone. The reversal of these zonal flows was apparently uncorrelated with seasonal forcing functions.

[41] From a Eulerian perspective, the absolute geostrophic velocity for upper 900 m was calculated by combining the float-observed hydrography and 900 m float parking-depth velocities. The absolute velocity fields showed good agreement with previous direct measurements, except for the heavy smoothing in the swift Gulf Stream region. We conclude that

[42] 1. Seasonal variability of the volume transport of the gyre for the upper 900 m was the maximum in winter and the minimum was in summer.

[43] 2. Eddy kinetic energy and eddy diffusivities in zonal and meridional directions at 900 m were calculated for each season. Spatially, the eddy variability peaked in the vicinity of the Gulf Stream, with the EKE 5–10 times larger in the Gulf Stream region than the interior of the recirculation gyre. Temporally, the eddy variability was a maximum in spring and minimum in winter near the Gulf Stream, but no apparent seasonal differences were found outside this region.

[44] The Argo project is now over half way towards its ambitious goal to cover the upper 2000 m of the world ocean with 3000 profiling floats (approximately 3° × 3° spatial resolution) with each float collecting CTD profiles at 10-day intervals [*Roemmich et al.*, 2001]. Argo will provide the approximately twice as many as profiles in our study region over a 5-year period as the number of profiles those were available for use in this study. The approach introduced in this study can eventually be applied to the Argo data in order to examine the structure of the absolute geostrophic velocity in the subtropical North Atlantic with enhanced resolution in both space and time, eventually
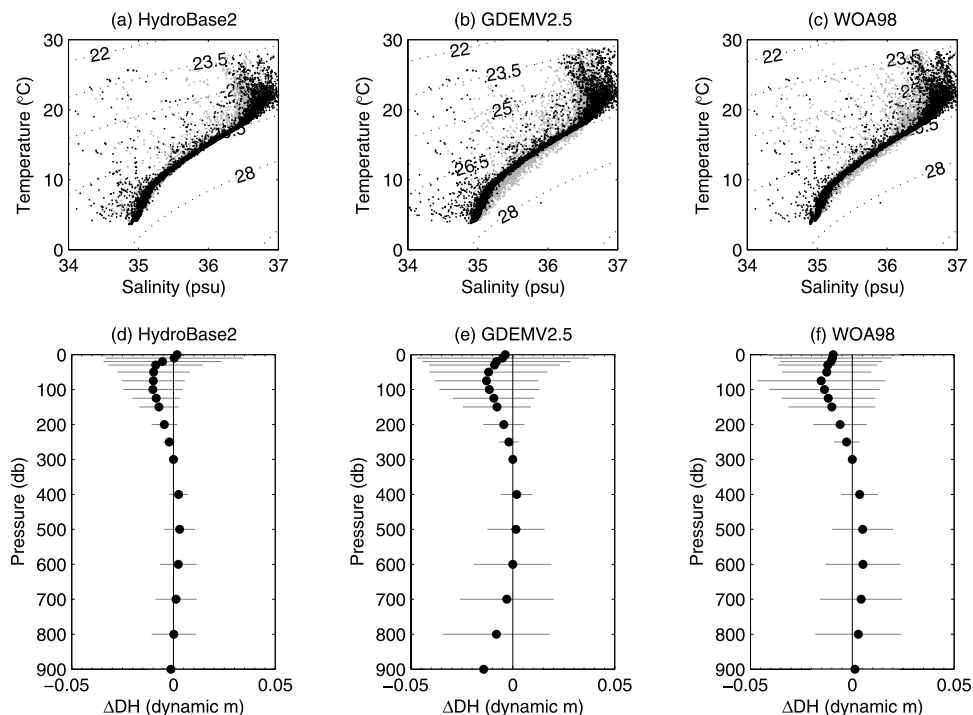
Figure A1. Assessment of estimated salinity based *T-S* relation from three different climatologies. (a, d) Based on Hydrobase2, (b, e) based on GDEMV2.5, and (c, f) based on WOA1998. (a–c) Black dots are *T-S* relations of 'observed *T*-observed *S*' from all the profiles of CTD floats, and gray dots are those of 'same observed *T*-estimated *S*' based on each climatology. (d–f) Mean and one standard deviation of the difference between dynamic heights from 'observed *T*-observed *S*' and 'observed *T*-estimated *S*'. Dynamic heights are calculated relative to 300 m.

improving on some of the results provided here for this most highly studied region of the world ocean.

## Appendix A: Salinity Estimation for Temperature-Only Profiles

[45] We compared three different climatologies for this purpose, i.e. HydroBase2, World Ocean Atlas 1998 (WOA98) [*Levitus et al.*, 1998], and the Generalized Digital Environmental Model Version 2.5 (GDEMV2.5) [*Teague et al.*, 1990]. These three climatologies were built based on different techniques. HydroBase2 was built on isopycnal averaging techniques [*Lozier et al.*, 1995], the WOA98 used optimal interpolation on depth surfaces [*Levitus et al.*, 1998], and the GDEMV2.5 was based on curve fitting of each profile [*Teague et al.*, 1990]. All three of climatologies provide monthly estimates. Both the *T-S* relation and pressure-salinity (*P-S*) relation from three climatologies were tested. The assessment was performed using the observed pairs of temperature and salinity profiles from CTD floats. For each observed CTD profile, an additional salinity was estimated from the each of the three climatologies and compared with the observed salinity. The estimated salinity profile was calculated by linear interpolation based on observed temperature (or pressure) and *T-S* (or *P-S*) relation from each climatology for the grid and month within which the observation was made. Figures A1a–A1c showed the *T-S* plots constructed using the observed temperature and salinity and analogous plots

using the observed temperature and the salinity derived from each climatology. Figures A1d–A1f show the mean and one standard deviation of the difference between the observed dynamic heights and the estimated dynamic heights at each standard depth. The estimated salinity for Figure A1 was calculated based on temperature-salinity relation. Similar comparisons were made based on *P-S* relationship, which produced larger discrepancies (not shown). The error in estimating dynamic height for the temperature-only profiles based on the *T-S* relation from HydroBase2 (used in the results reported in this paper) was found to be less than 0.01 dynamic meter for most of depths, with an envelope of uncertainty in the dynamic height calculation due to the estimation of salinity shown in Figure A1d.

Appendix B: Extrapolation of the Dynamic Height Profiles

[46] The shoaling of the float parking depth caused a significant decrease in the number of observations at the deeper levels (Figure B1). The upper 100 m also suffered from an insufficient number of observations. The salinity estimation was often unavailable because the *T-S* relation was not monotonic in this depth range, especially in winter. Thus, an additional vertical constraint was introduced to improve the vertical coherency of the objective mapping.

[47] First, all the dynamic height profiles were calculated relative to 300 m depth, and then the extrapolation using a
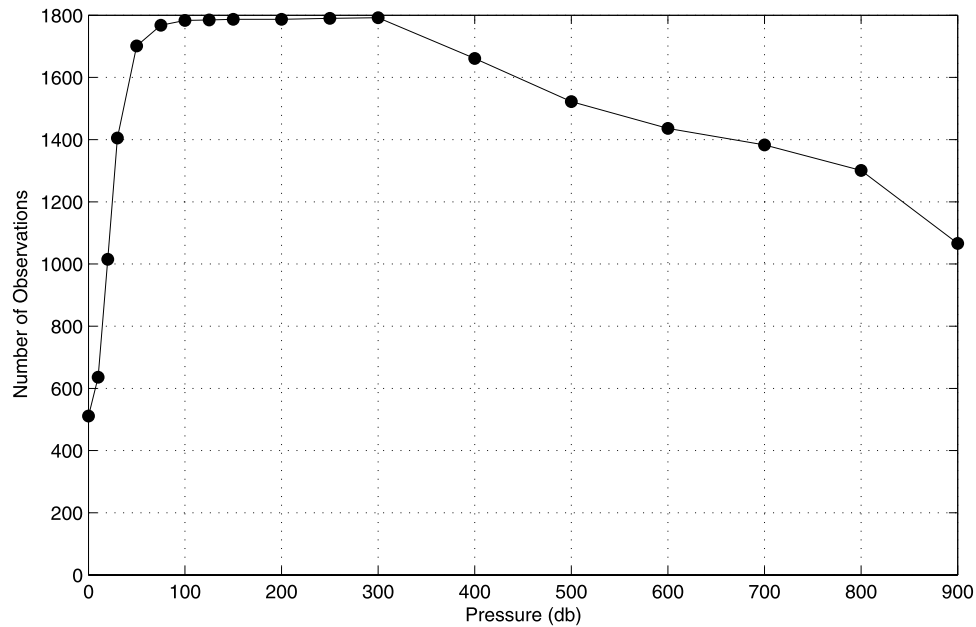
Figure B1. Number of dynamic height observations that were available for the objective mapping of each level for April–June.

second order polynomial fit was applied to each profile that failed to cover the full depth range (0–900 m). Then, all the dynamic height profiles were shifted to have 900 m as the level of no motion. The uncertainty in dynamic height calculation introduced from the extrapolation was assessed using the similar strategy to that of the salinity estimation. A segment of an observed dynamic height profile was used for the curve fitting and the remainder of the observed profile was compared with the estimated values from the extrapolation. Since the uncertainty of the extrapolation depends on the length of the observed profile, the assessments were carried out with various different lengths of segments from the observed profiles. For example, Figure B2 shows the mean and the standard deviation of the difference between observed dynamic heights and estimated dynamic heights using the segments that extend from 100 m to 500 m. As expected, the uncertainty increases at the deepest and the shallowest levels but is generally less than 0.1 dynamic meter. In the upper 100 m the extrapolation is biased toward the greater value, as it gets shallower. This is probably due to the fact that simple second order extrapolation cannot account for the existence of the surface mixed layer.

Appendix C: Error Estimation

[48] The major sources of uncertainty in the absolute velocity mapping procedure were the estimation of salinity for the temperature-only profiles, the extrapolation of dynamic height profiles, and the 10% local random error allowed in the objective mapping. All three uncertainties were estimated as previously explained, with the uncertainties given in terms of the equivalent dynamic height error. It is generally difficult to estimate the uncertainty in the velocity or the transport directly from the uncertainty of dynamic height field, because these uncertainties are related
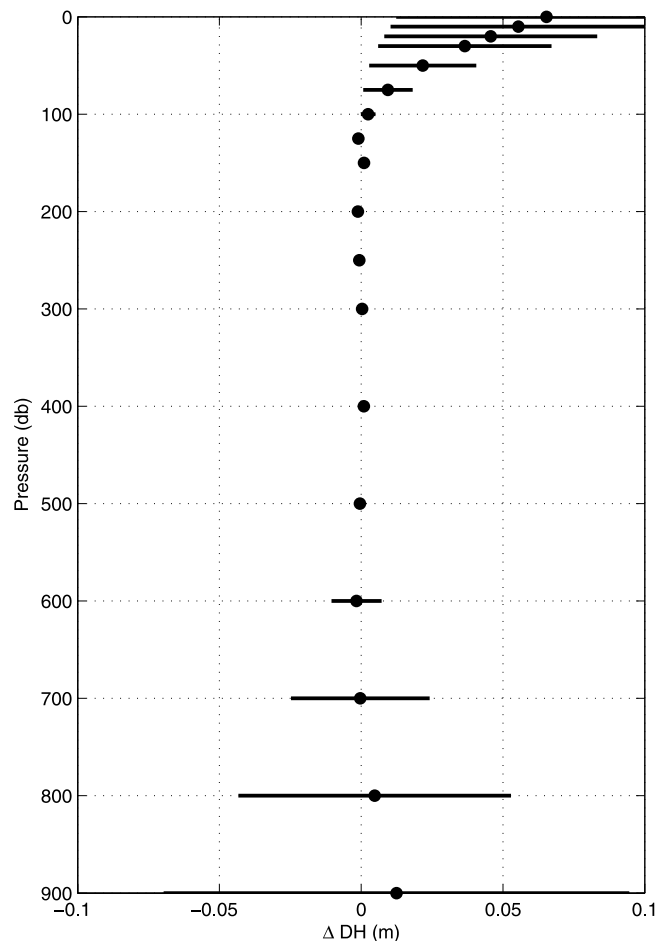
Figure B2. Example of the assessment of extrapolation of dynamic height profile. Mean and one standard deviation of difference between observed dynamic heights and extrapolated dynamic heights using 100–500 m segments of the observed dynamic height profiles.

not to the absolute magnitude of dynamic heights but to the horizontal gradient in the dynamic height field. Thus, adding estimated uncertainty uniformly to the dynamic height map would not produce any uncertainty in the geostrophic velocity field.

[49] To remedy this problem, the uncertainty in the absolute velocity was estimated in a Monté-Carlo fashion. Ten additional calculations were performed for each field using the identical procedures except for randomly adding estimated uncertainty at each step. For example, whenever the salinity was estimated for the temperature-only profile, the random uncertainty with the estimated mean and the standard deviation for each depth was added for ten additional sets of calculations. Uncertainty was also added in the same manner for every extrapolated dynamic height profile. For each objective mapping, 10% of the spatial variance of the original objectively mapped dynamic height field was randomly added, and then velocity was objectively mapped for the ten additional fields. These procedures were applied for both relative and reference velocity fields. Finally, ten additional absolute velocity fields were generated and averaged to produce estimated error. The resulting error was less than 1 cm/s for the most of the domain and most standard depths. The ten additional volume transports were also calculated from the ten additional absolute velocity fields and averaged to produce the estimated error in the volume transport as shown in Figure 18.

References

Boning, C. W. (1988), Characteristics of particle dispersion in the North Atlantic: An alternative interpretation of SOFAR float results, *Deep Sea Res.*, 35, 1379–1385.

Bower, A. S., B. Le Cann, T. Rossby, W. Zenk, J. Gould, K. Speer, P. L. Richardson, M. D. Prater, and H.-M. Zhang (2002), Directly measured mid-depth circulation in the northeastern North Atlantic Ocean, *Nature*, 419, 603–607.

Bretherton, F. P., R. E. Davis, and C. B. Fandry (1976), A technique for objective analysis design of oceanographic experiments applied to mode 73, *Deep Sea Res.*, 23, 559–582.

Carr, M.-E., and H. T. Rossby (2001), Pathways of the North Atlantic Current from surface drifter and subsurface floats, *J. Geophys. Res.*, 106, 4405–4419.

Clarke, R. A., H. W. Hill, R. F. Reiniger, and B. Warren (1980), Current systems south and east of the Grand Banks of Newfoundland, *J. Phys. Oceanogr.*, 10, 25–65.

Davis, R. E. (1987), Modeling eddy transport of passive tracers, *J. Mar. Res.*, 45, 635–666.

Davis, R. E., D. C. Webb, L. A. Regier, and J. Dufour (1992), The Autonomous Lagrangian Circulation Explorer (ALACE), *J. Atmos. Oceanic Technol.*, 9, 264–285.

Davis, R. E., J. T. Sherman, and J. Dufour (2001), Profiling ALACEs and other advances in autonomous subsurface floats, *J. Atmos. Oceanic Technol.*, 18, 982–993.

Ducet, N., P. Y. Le Traon, and G. Reverdin (2000), Global high-resolution mapping of ocean circulation from TOPEX/Poseidon and ERS-1 and −2, *J. Geophys. Res.*, 105(C8), 19,477–19,498.

Fischer, J., and F. A. Schott (2002), Labrador Sea water tracked by profiling floats - From the boundary current into the open North Atlantic, *J. Phys. Oceanogr.*, 32, 573–584.

Frantantoni, D. M. (2001), North Atlantic surface circulation during the 1990s observed with satellite-tracked drifters, *J. Geophys. Res.*, 106(C10), 22,067–22,093.

Freeland, H. J., P. B. Rhines, and T. Rossby (1975), Statistical observations of the trajectories of neutrally buoyant floats in the North Atlantic, *J. Mar. Res.*, 33, 383–404.

Fu, L.-L., J. Vazquez, and M. E. Parke (1987), Seasonal variability of the Gulf Stream from satellite altimetry, *J. Geophys. Res.*, 92(C1), 749–754.

Gould, W. J. (1985), Physical oceanography of the Azores front, *Prog. Oceanogr.*, 14, 167–190.

Halkin, D., and H. T. Rossby (1985), The structure and transport of the Gulf Stream at 73°W, *J. Phys. Oceanogr.*, 15, 1439–1452.

Hogg, N. G. (1992), On the transport of the Gulf Stream between Cape Hatteras and the Grand Banks, *Deep Sea Res.*, 39, 1231–1246.

Iselin, C. O. (1936), A study of the circulation of the western North Atlantic, *Pap. Phys. Oceanogr. Meteorol.*, 4, 1–101.

Joyce, T. M., A. Hernandez-Guerra, and W. M. Smethie Jr. (2001), Zonal circulation in the NW Atlantic and Caribbean from a meridional World Ocean Circulation Experiment hydrographic section at 66°W, *J. Geophys. Res.*, 106(C10), 22,095–22,113.

Kalnay, E., et al. (1996), The NCEP/NCAR 40-Year Reanalysis Project, *Bull. Am. Meteorol. Soc.*, 77, 437–471.

Kelly, K. A., S. Singh, and R. X. Huang (1999), Seasonal variations of sea surface height in the Gulf Stream region, *J. Phys. Oceanogr.*, 29, 313–327.

Krauss, W. (1986), The North Atlantic Current, *J. Geophys. Res.*, 91, 5061–5074.

Lavender, K. L., R. E. Davis, and W. B. Owens (2000), Mid-depth recirculation observed in the interior Labrador and Irminger Seas by direct velocity measurements, *Nature*, 407, 66–69.

Lee, T., and P. Cornillon (1995), Temporal variation of meandering intensity and domain-wide lateral oscillations of the Gulf Stream, *J. Geophys. Res.*, 100(C7), 13,603–13,613.

Le Traon, P. Y. (1990), A method for optimal analysis of fields with spatially variable mean, *J. Geophys. Res.*, 95(C8), 13,543–13,547.

Levitus, S., T. P. Boyer, M. E. Conkright, T. O'Brien, J. Antonov, C. Stephens, L. Stathoplos, D. Johnson, and R. Gelfeld (1998), *World Ocean Database 1998*, vol. 1, *Introduction*, NOAA Atlas, NESDIS 18, 346 pp, U.S. Govt. Print. Off., Washington, D. C.

Lozier, M. S., W. B. Owens, and R. G. Curry (1995), The climatology of the North Atlantic, *Prog. Oceanogr.*, 36, 1–44.

Lumkin, R., A.-M. Treguier, and K. Speer (2002), Lagrangian eddy scales in the northern Atlantic Ocean, *J. Phys. Oceanogr.*, 32, 2425–2440.

McWilliams, J. C. (1976), Maps from the Mid-Ocean Dynamics Experiment: part I. Geostrophic streamfunction, *J. Phys. Oceanogr.*, 6, 810–827.

Owens, W. B. (1991), A statistical description of the mean circulation and eddy variability in the northwestern Atlantic using SOFAR floats, *Prog. Oceanogr.*, 28, 257–303.

Park, J.-J., K. Kim, B. A. King, and S. C. Riser (2005), An advanced method to estimate deep currents from profiling floats, *J. Atmos. Oceanic Technol.*, in press.

Perez-Brunius, Paula, T. Rossby, and D. R. Watts (2004), Absolute transports of mass and temperature for the North Atlantic Current-Subpolar Front System, *J. Phys. Oceanogr.*, 34, 1870–1883.

Poulain, P.-M., A. Warn-Varnas, and P. P. Niiler (1996), Near-surface circulation of the Nordic seas as measured by Lagrangian drifters, *J. Geophys. Res.*, 101(C8), 18,237–18,258.

Qiu, B. (1994), Determining the mean Gulf Stream and its recirculations through combining hydrographic and altimetric data, *J. Geophys. Res.*, 99, 951–962.

Reid, J. L. (1978), On the middepth circulation and salinity field in the North Atlantic Ocean, *J. Geophys. Res.*, 83(C10), 5063–5067.

Reverdin, G., P. P. Niiler, and H. Valdimarsson (2003), North Atlantic Ocean surface currents, *J. Geophys. Res.*, 108(C1), 3002, doi:10.1029/2001JC001020.

Richardson, P. L. (1981), Gulf Stream trajectories measured with free-drifting buoys, *J. Phys. Oceanogr.*, 11, 999–1010.

Richardson, P. L. (1983), Eddy kinetic energy in the North Atlantic from surface drifters, *J. Geophys. Res.*, 88, 4355–4367.

Richardson, P. L. (1985), Average velocity and transport of the Gulf Stream near 55°W, *J. Mar. Res.*, 43, 83–111.

Richman, J. G., C. Wunsch, and N. G. Hogg (1977), Space and time scales of mesoscale motion in the western North Atlantic, *Rev. Geophys.*, 15, 385–420.

Riser, S. C. (1982), The quasi-Lagrangian nature of the SOFAR floats, *Deep Sea Res.*, 29, 1587–1602.

Roemmich, D., et al. (2001), Argo: The global array of profiling floats, in *Observing the Oceans in the 21st Century*, edited by C. J. Koblinsky and N. R. Smith, pp. 248–258, Bur. of Meteorol., Melbourne, Victoria, Australia.

Roemmich, D., S. Riser, R. Davis, and Y. Desaubies (2004), Autonomous profiling floats: Workhorse for broad-scale ocean observations, *Mar. Technol. Soc. J.*, *38*, 21–29.

Rossby, H. T. (1996), The North Atlantic Current and surrounding waters: At the crossroads, *Rev. Geophys.*, *34*, 463–481.

Rossby, H. T., and E. Gottlieb (1998), The Oleander Project: Monitoring the variability of the Gulf Stream and adjacent waters between New Jersey and Bermuda, *Bull. Am. Meteorol. Soc.*, *79*, 5–18.

Rossby, H. T., and H.-M. Zhang (2001), The near-surface velocity and potential vorticity structure of the Gulf Stream, *J. Mar. Res.*, *59*, 949–975.

Rossby, H. T., S. C. Riser, and A. J. Mariano (1983), The western North Atlantic - A Lagrangian viewpoint, in *Eddies in Marine Science*, edited by A. R. Robinson, 609 pp., Springer, New York.

Sato, O. T., and T. Rossby (1995), Seasonal and low frequency variations in dynamic height anomaly and transport of the Gulf Stream, *Deep Sea Res.*, *42*, 149–164.

Schmitz, W. J., Jr., and W. R. Holland (1986), Observed and modeled mesoscale variability near the Gulf Stream and Kuroshio Extension, *J. Geophys. Res.*, *91*(C8), 9624–9638.

Spall, M. A., P. L. Richardson, and J. Price (1993), Advection and eddy mixing in the Mediterranean salt tongue, *J. Mar. Res.*, *51*, 797–818.

Stammer, D., and C. Wunsch (1999), Temporal changes in eddy energy of the oceans, *Deep Sea Res., Part II*, *46*, 77–108.

Stommel, H., P. Niiler, and D. Anati (1978), Dynamic topography and recirculation of the North Atlantic, *J. Mar. Res.*, *36*, 449–468.

Teague, W. J., M. J. Carron, and P. J. Hogan (1990), A comparison between the Generalized Digital Environmental Model and Levitus climatologies, *J. Geophys. Res.*, *95*(C5), 7167–7183.

Watts, D. R. (1983), Gulf Stream variability, in *Eddies in Marine Science*, edited by A. R. Robinson, 609 pp., Springer, New York.

Worthington, L. V. (1976), *On the North Atlantic Circulation*, 110 pp., Johns Hopkins Univ. Press, Baltimore, Md.

Wunsch, C., and D. Stammer (1998), Satellite altimetry, the marine geoid, and the oceanic general circulation, *Annu. Rev. Earth Planet. Sci.*, *26*, 219–253.

—————————————

Y.-O. Kwon, Climate and Global Dynamics Division, National Center for Atmospheric Research, Boulder, CO 80305, USA. (yokwon@ucar.edu)

S. C. Riser, School of Oceanography, University of Washington, Seattle, WA 98195, USA.